How conspicuous are peacock eyespots and other colorful feathers in the eyes of mammalian predators?

Suzanne Amador Kane[1*], Yuchao Wang[1], Rui Fang[1] , Yabin Lu[1] , Roslyn Dakin[2]

[1] Physics & Astronomy Department, Haverford College, Haverford, PA, USA

[2] Migratory Bird Center, Smithsonian Conservation Biology Institute, National Zoological Park, Washington, DC, USA

*corresponding author

Email: samador@haverford.edu

Short title: Are colorful feathers conspicuous in the eyes of mammalian predators?

Keywords: color vision, predation, feather, multispectral imaging, camouflage, distance

Abstract

Feathers perceived by humans to be vividly colorful are often presumed to be equally conspicuous to other mammals, and thus to present an enhanced predation risk. However, many mammals that prey on adult birds have dichromatic visual systems with only two types of color-sensitive visual receptors (one sensitive to ultraviolet light), rather than the three characteristic of humans and four of most birds. Thus, understanding how these predators perceive color requires quantitative visual modeling. Here, we use a combination of reflectance spectroscopy, multispectral imaging, color vision modelling and visual texture analysis to compare the visual

signals available to conspecifics and to mammalian predators for multicolored feathers from the Indian peacock (*Pavo cristatus*) as well as red and yellow parrot feathers; we also take into account the effects of distance-dependent blurring due to visual acuity. When viewed by tetrachromatic birds against a background of green vegetation, most of the feathers studied had color and brightness contrasts similar to values previously found for ripe fruit. By contrast, when viewed by dichromat mammalian predators, the color and brightness contrasts of these feathers were only weakly detectable and often did not reach detection thresholds for typical viewing distances. We furthermore show that the peacock's erect train has undetectable color and brightness contrasts and visual textures when photographed against various foliage backgrounds. Given the similarity of photoreceptor sensitivities and feather reflectance properties across relevant species, these findings are consistent with many feathers of similar hue being inconspicuous, and in some cases potentially cryptic, in the eyes of their mammalian predators. These results suggest that many types of colorful feathers are likely to be cryptic to mammals while providing a communication channel perceptible to birds, while emphasizing the importance of understanding diverse sensory receivers in the evolution of animal coloration.

Introduction

Ever since Darwin, colorful feathers such as the iridescent eyespots of the Indian peacock (*Pavo cristatus*) (Fig 1A) have been assumed to present salient visual signals readily detectable by their natural predators (Darwin, 1888; Ranjith and Jose, 2016; Ruxton et al., 2004). For this reason, these sexually-selected ornaments have been proposed to incur a cost due to increased predation. For example, as Zahavi stated in his paper introducing the handicap principle: "The more brilliant the plumes, the more conspicuous the male to predators" (Zahavi, 1975). Evidence for

such countervailing selection pressures has been found in ornamented guppies preyed upon by fish (Endler, 1980) and in birds preyed upon by other birds (Møller and Nielsen, 2006). However, while this assumption is predicated on the predator being able to detect prey visual signals (Outomuro et al., 2017), no studies have tested whether this is true for the mammalian predators that prey on many birds. For example, the primary predators of adult peafowl are carnivorans (felids and canids, S1 Appendix), which all have dichromatic visual systems; i.e., they have only two types of cone visual receptors with distinct spectral sensitivities, not the four characteristic of most birds (Cronin et al., 2014) or the three found in most humans. More generally, felids (e.g., *Felis catus*) are a major threat to bird populations world-wide (Loss et al., 2015). Because dichromatic mammals lack red-green color discrimination, they are unlikely to detect many of the chromatic visual cues evident to birds and humans (Cronin et al., 2014; Miller and Murphy, 1995). Studies of visual ecology have considered how prey appear to various types of predators (birds, insects and fish) for many types of prey, including insects and birds (Håstad et al., 2005; Théry et al., 2005), fish (Endler, 1991), cuttlefish (Chiao et al., 2011), crustaceans (Nokelainen et al., 2017), primates (Sumner and Mollon, 2003) and lizards (Outomuro et al., 2017). Two previous studies also have studied the iridescence reflectance spectra of peacock eyespots and how they are perceived by peahens (females) (Dakin and Montgomerie, 2013; Loyau et al., 2007). As yet, no studies have compared how visual signals from peacocks and other avian prey appear in the vision of their mammalian predators.

Fig 1. Peacocks and the model peacock train. A) An Indian peacock displaying his erect train to a peahen (female) in the foreground and B) another individual holding his train folded while

68 walking. C) Model peacock train assembled from a collection of eyespot feathers used to
69 evaluate the appearance of the train viewed against vegetation.
70
71
72 During courtship displays, male Indian peafowl ("peacocks") attract mates by spreading, erecting
73 and vibrating the fan-like train ornament (Fig. 1A), causing it to shimmer iridescently and emit
74 mechanical sound (Dakin and Montgomerie, 2009; Dakin et al., 2016; Freeman and Hare, 2015).
75 Several lines of evidence indicate that these feathers are assessed during mate choice: train-
76 rattling performance by peacocks is obligatory for mating success (Dakin and Montgomerie,
77 2009), eye-tracking experiments have shown that train-rattling displays are effective at attracting
78 and holding the peahen's gaze (Yorzinski et al., 2013), and eyespot iridescence has been shown
79 to account for approximately half of variation in male mating success (Dakin and Montgomerie,
80 2013; Loyau et al., 2007). Because peacocks spend the majority of their time in activities other
81 than courtship displays even during the breeding season (Dakin and Montgomerie, 2009;
82 Harikrishnan et al., 2010), any test of visual saliency must also consider the appearance of the
83 folded train. Furthermore, because the peacock's head, neck and breast are covered by iridescent
84 blue contour feathers (Yoshioka and Kinoshita, 2002), the visual cues generated by this body
85 plumage are also relevant for salience to potential mates and predators.
86
87 Here, we use multispectral imaging and reflectance spectroscopy to compare how detectable
88 peacock feathers are to conspecifics and dichromatic mammalian predators (hereafter
89 "dichromatic mammals"), as measured by color, brightness, and texture contrast relative to green
90 background vegetation, following similar studies of prey that utilize camouflage against

predators with a variety of visual systems (Stevens and Merilaita, 2011). Our goal was to test the assumption that colorful feathers that are highly conspicuous to conspecific birds are also readily detectable by these predators. To determine how generalizable our results were to other hues of colorful plumage, we also measured reflectance spectra and multispectral images of red and yellow parrot feathers. We then used psychophysical vision models to test whether conspecifics and dichromatic mammalian predators can readily detect the color and brightness contrasts between feathers and green vegetation. Our analysis modeled the appearance of feathers at various distances to determine when each observing species could distinguish color patches relative to the surrounding environment.

In addition to color cues, visual salience depends on the presence of pattern features that are perceptually discriminable from the background. To determine whether predators might detect the peacock's train using such visual texture cues, we analyzed images of the model train relative to that of background vegetation using two pattern analysis methods motivated by visual processing in vertebrates (Stoddard and Stevens, 2010). Granularity analysis is a spatial filtering method that determines the contributions to image contrast of features with different sizes; this image processing technique has been used to compare pattern textures in studies of cephalopod, avian egg, fish and shore crab camouflage, as well as humans searching for objects against various backgrounds (Akkaynak et al., 2017; Barbosa et al., 2008; Nokelainen et al., 2017; Stoddard and Stevens, 2010; Troscianko et al., 2017). A second method, edge detection, provides a complementary measure of texture complexity by using image processing to detect sharp gradients in intensity (Stoddard et al., 2016).

Materials and methods

Feather samples

Five Indian peafowl eyespot (Fig 2A), three blue peacock contour breast feathers (Fig 2B), four scarlet macaw (*Ara macao*) wing feathers (two red and six yellow patches total) (Fig 3A), two Amazon parrot wing feathers (two red and two yellow patches total) (Fig 3B), and four red African grey parrot (*Psittacus erithacus*) tail feathers (Fig 3C) were obtained from Moonlight Feather (Ventura, CA USA) and Siskiyou Aviary (Ashland, OR USA). Because the psittacofulvin pigments in parrot feathers have reflectance spectra with similar spectral features to red and yellow carotenoid pigments (Shawkey and Hill, 2005; Toral et al., 2008), our results should be representative of red and yellow feathers in general. Our number of replicates for the peacock eyespots agree well with recommendations from a study of intraspecies variations in feather color measures (Dalrymple et al., 2015); however, we were limited by availability to fewer replicates for the parrot feathers. For mounting, eyespot feathers were cut off below the outermost colored ring at the proximal end. All feather types were mounted on black matte art quality paper with a magnetic backing that adhered to the tilt stages used for spectroscopy and multispectral imaging. Feather samples were stored without compression in sealed boxes in acid-free envelopes at 75% relative humidity and ambient temperature (22 ± 2 deg C). The different peacock eyespot color patches (colored rings and central disk) are referred to using the names and two letter abbreviations indicated in Fig 2A.

Fig 2. Peafowl cone sensitivity spectra and peacock feather vs green vegetation reflectance spectra. (A) An Indian peacock eyespot feather showing the color patch names used in the analysis. (B) Peacock blue breast plumage. (C) Comparison of the cone photoreceptor spectral

sensitivities for the Indian peafowl and ferret, which has dichromatic color vision very similar to that of cats and dogs. All spectra are multiplied by the D65 illuminance spectrum used to model sunlight and normalized to unit area. Reflectance spectra of (D) peacock feather eyespots and (E) peacock iridescent blue body plumage and the green saucer magnolia (*Magnolia x soulangeana*) leaf used as a background for the feather sample images.

Fig 3. Parrot feather images, cone sensitivity spectra and feather reflectance spectra. (A) Scarlet macaw, (B) Amazonian parrot and (C) African grey parrot feather samples. (D) Comparison of the cone photoreceptor spectral sensitivities for the blue tit, which has tetrachromatic ultraviolet sensitive (UVS) color vision similar to that of parrots, and the ferret, which has dichromatic color vision similar to that of cats and dogs. All spectra are multiplied by the D65 illuminance spectrum used to model sunlight and normalized to unit area. (E) Reflectance spectra of the parrot feather red and yellow patches studied here.

We also assembled an array of 28 peacock feathers (Fig 1C) to create a model train arranged to match the geometry of eyespots in actual peacock trains ((Dakin and Montgomerie, 2013)); this was used to simulate the appearance of the train during display (when the train is erect) or during walking, perching or standing (when the train is held horizontally; see Fig 1B). In their native range in India and Pakistan, peafowl are reported to live in a variety of habitats, including open moist and dry-deciduous forest, scrub jungle, and adjacent grasslands, and their breeding season is reported to coincide with the start of the rainy season (Gokula, 2015), after which eyespot feathers are shed by molting (Beebe, 1918; Sharma, 1974). We used as background foliage for feather and model train images various plants (grass, brush and trees) native to the northeast

USA (S2 Appendix). Because green flora have generic reflection spectra due to chlorophyll absorption (Jensen, 2009), the plants used in this study should be representative of the color and luminance of those found in the native environments of peafowl and many other bird species.

Vision models

The Indian peafowl's visual system has four classes of color-sensitive (chromatic) single cone cells: violet (VS), short (SWS), medium (MWS) and long (LWS) wavelength-sensitive cones, and one type of double cone that is sensitive to brightness (luminance) (Hart, 2002). In order to illustrate their spectral responses under natural illumination, Fig 2C shows the peafowl cone's spectral sensitivities $S_r(\lambda)$ for the r^{th} photoreceptor type (including ocular media and oil droplet transmission) multiplied by the CIE D65 irradiance spectrum, $I(\lambda)$, and normalized to unit area; we used this standard illuminant because of its close match the solar irradiance spectrum for the elevation angles found for actual peacock displays (Dakin and Montgomerie, 2009; Spitschan et al., 2016). To model the tetrachromatic UVS (ultraviolet-sensitive) vision of parrots we used blue tit (*Cyanistes caeruleus*) cone spectral sensitivities (Hart et al., 2000; Troscianko and Stevens, 2015). (Fig 3D).

The visual systems of dichromatic mammalian predators have been studied for a variety of genera, and found to include S (blue- to near-UV-sensitive) (Douglas and Jeffery, 2014) and L (green-sensitive) cone populations in all carnivorans studied to date, including felids (Guenther and Zrenner, 1993) and canids (Jacobs et al., 1993). Behavioral studies have confirmed that domestic cats (Clark and Clark, 2016) and dogs (Kasparson et al., 2013; Neitz et al., 1989) have dichromatic color vision. Brightness signals in dichromatic mammals are assumed to be due to

only the L cones (Osorio and Vorobyev, 2005). We used ferret (*Mustela putorius*) cone spectra (Troscianko and Stevens, 2015) to model dichromat vision because ferret spectral peaks agree closely with those of cats and dogs (i.e., ≤ 4.4% for S and ≤ 1.4% for L cones) (Calderone and Jacobs, 2003; Guenther and Zrenner, 1993; Jacobs et al., 1993) (Fig 2C). While many carnivorans are primarily nocturnal or crepuscular, at low light levels, photopic chromatic signals will be weak and visual signals will be dominated by luminance contrast via rods or double cones. Thus, we consider high luminance photopic conditions as the best case scenario for visual detection by these predators.

Multispectral imaging

Multispectral images were recorded using a GoPro Hero 4 Silver Edition camcorder (GoPro Inc, San Mateo, CA USA) modified for full spectral imaging by replacing its original lens and infrared (IR) filter with a quartz lens transparent to < 300 nm (Igoe et al., 2013; Prutchi, 2016). Because the spectral response of this camera's IMX117 Exmor-R CMOS sensor (Sony Corp., Tokyo, Japan) is sensitive throughout the visible and near-UV, these cameras have been used in multispectral imaging (Vogt and Vogt, 2016; Yun et al., 2016) (S1 Fig). Multispectral photographs were recorded at 3000 × 2250 pixel resolution and the GoPro settings medium field of view, Protune CAM-RAW mode (for no white balance compensation), flat color, low sharpness, ISO 400, exposure -2, night mode (to enable shutter speed control), auto shutter and spot meter on. Each sample was photographed for each geometry and illumination condition to give two multispectral images: 1) a UV image using an Andrea-UV filter (< 1% transmission for > 400 nm; UVIROptics, Eugene, Oregon USA; 2) a visible RGB (red, green, blue) image using two UV-IR cut filters to pass 400-700 nm light (Hoya Corp., Tokyo Japan). Filter transmission

spectra were measured using the methods described below in "Reflectance Spectroscopy" (S1 Fig). The camera's large depth-of-field eliminated the need for refocusing between visible and UV images. To maintain constant camera alignment between photographs, we mounted the camera rigidly using optical mounts (Thorlabs, Newton NJ, USA) and attached filters using quick-release Xume magnetic adapters (Panalpina Inc., Port Reading, NJ, USA); all images were taken using a remote trigger. Each feather image included a model Micro FSS08 8-step grayscale diffuse reflectance standard (Avian Technologies, New London, NH USA) mounted level with the sample plane for calibrating absolute reflectance (Troscianko and Stevens, 2015). Images of the model train included a larger 6-step grayscale and color checker chart (DGK Color Tools WDKK Waterproof, Digital Image Flow, Boston MA USA). Reflectance spectra for each grayscale in each filter and camera color channel combination were measured using the methods described below in "Reflectance Spectroscopy". Each image also included an object of known size for spatial calibration.

All samples were mounted on a tripod for imaging (S2 Fig). Three sets of multispectral images each were obtained with the model train held erect and held horizontal viewed from the side. Peacock eyespots were oriented with their rachis vertical to simulate their average orientation in the erect train during courtship displays and the model train was oriented in a variety of directions to simulate the variation in appearance of the iridescent train eyespot feathers during courtship display, standing and walking. The camera was mounted on a second tripod a distance 20.0 ± 1.0 cm from feather samples and 1.70 to 2.00 ± 0.05 m from the model train. For feather samples, the camera was oriented to record images at normal observation angle ($\theta = 0 \pm 2$ deg) with respect to the feather sample plane (Fig 4). The size of feather sample images was 55 mm x

67 mm, corresponding to 7.3 pixel/mm. Images were captured during June-July 2018 in the Haverford College Arboretum (latitude, longitude: 40.0093° N, 75.3057° W) for 24.2 ± 0.2 deg C and 55.5 ± 1.5 % relative humidity. All feather samples were illuminated by direct sunlight with an azimuthal angle $\Psi = 45 \pm 3$ deg clockwise from the camera's optical axis and at solar elevation angles $\Phi = 30 \pm 3$ deg, corresponding to an angle $\alpha = 52 \pm 3$ deg between the observation and illumination directions (Fig 4). These illumination and observation angles agree with those measured for female peafowl observing courtship displays (Dakin and Montgomerie, 2009). In general, these solar angles hold for the early morning times when most birds are most active (Robbins, 1981). Optimal color contrasts for non-iridescent feathers have been found to correspond to the range of observation-illumination angles α used in this study (Barreira et al., 2016); this is relevant because pigment-based colors can appear in combination with structural coloration (Shawkey and Hill, 2005). Furthermore, for this observation geometry, the bird's body subtends the greatest visual angle. The peacock eyespot feather samples were surrounded by additional loose green barbs to simulate their setting in the actual train, while the parrot feather samples were surrounded by a saucer magnolia leaves picked ≤ 1 hour before image capture. We also imaged a variety of green leaves for comparison (S3 Fig). Black velvet fabric was mounted behind the feather samples to limit backscattered light and a lens hood was used to reduce lens flare. The model peacock train was photographed against a variety of foliage backgrounds for solar elevation angle between 37 to 55 deg.

Fig 4. Multispectral imaging geometry showing the angles of observation and illumination.

Multispectral images were first processed using custom scripts written in MATLAB v15a with the Machine Vision, Signal Processing and Fitting toolboxes (MathWorks, Natick MA USA); all code is available on figshare at https://figshare.com/s/f8add694af9c79de7f76. Images stored as jpeg files were calibrated and corrected for lens distortions using the MATLAB Camera Calibration application, and then corrected for perspective distortions using MATLAB's *fitgeotrans* and *imwarp* commands. Images captured using the UV and visible filters were checked for alignment by hand and then converted into linearized and normalized measures of reflectance, as explained under "Quantitative visual signal analysis" below.

To account for distance-dependent blurring due to each viewing species' visual acuity (Barnett et al., 2018; Caves and Johnsen, 2018), multispectral images with linearized intensities were spatially filtered before analysis to model the effect of viewing distance on contrasts between feathers and background foliage, and its effect on contrasts within the patterned eyespot feathers (See details in S3 Appendix). While peahens view peacock courtship displays at nearby distances $\geq$ 1 to 2 m (Dakin and Montgomerie, 2009), we also modeled a variety of greater viewing distances (2, 4, 8 and 16 m). Color patches were defined by hand in the original images and used for each modeled distance for uniformity. After spatial filtering and before color and brightness analysis, we sampled intensity values in the multispectral images on a square grid with spacing equal to a visual acuity disk, following (Endler, 2012). To model the effect of spatial filtering on the peacock's blue head, neck and breast plumage, we used an image with green foliage background with an approximately peacock-shaped cutout of the blue plumage superimposed; spatial filtering was performed using peacock body dimensions (Talha et al., 2018) to define the composite image's effective spatial scale.

To approximate how the feathers appear in each viewer's visual system, three type of false color images (ultraviolet, human visible RGB and viewer false color) were created from the multispectral images in MATLAB using square-root transformed cone quantum catches, Q_{pr} normalized to the maximum value of the brightest cone quantum catch on each image. To represent the tetrachromatic vision of peafowl, an RGB image was created from the computed LWS, MWS and SWS data, respectively and a magenta image was created using the VS cone data. To model dichromatic mammalian predator vision, we made up a single false color image using blue to represent the S cone and yellow to represent the L cone quantum catch values.

Reflectance spectroscopy

We measured reflectance spectra using a model USB2000+ spectrometer and OceanView software (Ocean Optics, Largo FL, USA) over the wavelength range 300–850 nm, using 100 ms integration time, 3 pixel boxcar averaging (corresponding to the optical resolution of 6.5 pixels = 2.06 nm FWHM), and averaging over 5 samples. All spectra were recorded in a dark room. Samples were illuminated by an Ocean Optics PX-2 Pulsed Xenon Light source triggered at 200 Hz using square wave pulses from a model 330120A function generator (Agilent Technologies, Wilmington, DE, USA); the source was turned on and allowed to warm up and stabilize for 15 minutes before data collection. Light for illumination and detection was carried in P400-1-UV-VIS optical fibers transparent to 200 nm (Ocean Optics). We used two PTFE white standards with flat 99.0% reflectance over 300-700 nm: a Spectralon USRS-99-010-EPV (Labsphere, North Sutton, NH USA) and a model SM05CP2C (Thorlabs). White standard and dark currents were measured every fifteen minutes. For each feather and each measurement geometry, raw

297 reflectance spectral data were recorded for each feather color patch sample radiance, AR, white
298 standard radiance, AR_r and dark current, D. The reflectance spectrum, $R(\lambda) = \frac{AR - D}{AR_r - D}$, was
299 smoothed over a wavelength interval of 20 nm using Savitzky-Golay smoothing in Origin; this
300 reduced high frequency noise but did not change reproducible features of the spectra peak
301 shapes.
302
303 Transmission spectra for the filters used in multispectral imaging were measured by recording
304 the spectrum of light reflected from the white standard with and without the filter inserted into
305 the light path with its face at normal incidence to the incident light. Reflectance values for color
306 and gray standards were measured using a RPH-SMA reflectance probe stand (Thorlabs, Newton
307 NJ USA) with the illuminating light at 45 deg to normal incidence and detected at normal
308 incidence. The reflectance goniometer for feather measurements used (S2 Fig) was adapted from
309 previously published designs (Van Wijk et al., 2016) (S2 Fig) but with an additional angular
310 degree of freedom to allow measurement of the bidirectional reflectance distribution function, in
311 which the angle of observation and illumination are not confined to the specular reflection
312 geometry (Vukusic and Stavenga, 2009). Both the illumination and detection optical pathways
313 were focused using a 74-UV lens (Ocean Optics) to a 2 mm diameter spot at about 5 cm from the
314 output surface of the lens. The feather samples were realigned every time the angle of
315 illumination and/or detection was adjusted to ensure both beams focused on the same region of
316 the feather. To assess reproducibility of spectra for the same color patch on each feather, we
317 measured each set of spectra three times for each sample after dismounting and remounting each
318 sample.
319

Quantitative visual signal analysis

We computed the color contrast, ΔS_c, between color patches in the feathers and background vegetation in our multispectral images using the receptor noise limited color opponent model, which has been shown to predict behavioral thresholds for visual signals in birds, humans and insects (Vorobyev and Osorio, 1998). All calculations were performed using a custom MATLAB script, which was tested by verifying that it computed the same values as the multispectral analysis software package MICA version 1.22 (Troscianko and Stevens, 2015). First, intensity values, V, from each multispectral image were corresponded to the actual reflected irradiance, R, for this camera by an S-log transformation:

$$R(V) = Ae^{-\frac{V}{T_o}} + C. \quad (1)$$

The parameters A, T_o and C were obtained from nonlinear least squares fits in MATLAB (adjusted-$R^2 \geq 0.997$) of the measured V and R values for each pixel in each RGB channel of the image. The resulting fits then were used to convert measured intensity values for each p^{th} color patch into linearized and normalized reflected intensities (range [0,1]) for each combination of filter and RGB image channel. To compute the color and brightness contrasts, these intensities were converted into the cone quantum catch values, Q_{pr}, for each of the viewer's r^{th} cone photoreceptors:

$$Q_{pr} = \int I(\lambda) R_p(\lambda) S_r(\lambda) d\lambda / \int I(\lambda) S_r(\lambda) d\lambda \,, \quad (2)$$

where $I(\lambda)$ is the illumination spectrum, $S_r(\lambda)$ is the r^{th} cone receptor's normalized spectral sensitivity and $R_p(\lambda)$ is the pth patch's reflectance spectrum. Because birds and mammals are known to achieve color constancy under a wide variety of illumination conditions (Kelber and Osorio, 2010; Olsson et al., 2016), this equation also incorporates the von Kries transformation, a mechanism for maintaining color constancy (Stoddard and Prum, 2008). To accomplish this

conversion, we used MICA to compute the parameters of a polynomial cone mapping between the UV blue channel and the visible RGB channels of the multispectral images recorded by our filter-camera system and the corresponding cone quantum catches, Q_{pr} (Stevens et al., 2007). This software finds the optimal mapping using our measured filter transmission and camera RGB spectral response curves with either the dichromatic ferret or tetrachromatic peafowl cone spectral sensitivities, the CIE D65 illumination spectrum and a large database of natural spectra. The net effect is to combine all measured values of linearized and normalized reflectance to compute the quantum catch, Q_{pr}, of each r^{th} cone (r = S or L for dichromats and r = VS, SWS, MWS, or LWS for tetrachromats) for the p^{th} sample color patch. Using a linear 2-way interaction cone mapping model, we obtained a near perfect fit for each visual system: ferret ($R^2 \geq 0.999$), peafowl ($R^2 \geq 0.996$) and blue tit (≥ 0.990 UVS cone, ≥ 0.998 all other cones).

The resulting cone quantum catch values, Q_{pr}, can be used to compute normalized color space coordinates, for the pt^h color patch: $q_p = \frac{Q_{pr}}{\sum_r Q_{pr}}$. For tetrachromats, the receptor index r = VS or UVS, SWS, MWS, LWS and q_p = (v,s,m,l), while for dichromats r = S, L and q_p = (sw,lw). After normalization, this corresponds to a three-dimensional tetrachromat color space for birds and a one-dimensional colorspace for dichromats, here chosen to rely on sw. To validate the results of our multispectral imaging code, we compared dichromat color space sw coordinates computed by both MICA and our MATLAB code (sw_M) from our multispectral images with those computed directly from reflectance spectra (sw_R) for six color chart squares. Use of the camera and UV/visible filter cone mapping model was validated for multispectral image analysis by the goodness of the linear fit, zero intercept and unit slope, between the two sets of color

space measures gave $sw_M = (0.018 \pm 0.031) + (1.00 \pm 0.07) \times sw_R +$ (adjusted-$R^2 = 0.993$) (S1 Fig).

To compute color contrasts, ΔS_c, we first computed the r[th] cone's log-linear quantum catch (Weber-Fechner), log Q_{rp}, for each p[th] patch. This was used to compute the difference in r[th] cone response for the pq[th] patch pair, $\Delta_{rpq} = \log Q_{rp} - \log Q_{rq}$. The color contrast then is computed from differences between opponent cone pairs weighted by receptor noise. Dichromats have only S/L receptor opponency, so for them, $\Delta S_C = \left|\Delta_{Lpq} - \Delta_{Spq}\right| \Big/ \sqrt{e_L^2 + e_S^2}$ (Vorobyev and Osorio, 1998). The corresponding equation for color contrast in tetrachromats is more complicated because all six possible combinations of the four single cones pairs should be considered (Kelber, 2016):

$$\Delta S_C^2 = \frac{\left(\begin{array}{l}\left(e_S e_{VS}\right)^2\left(\Delta_L - \Delta_M\right)^2 + \left(\left(e_M e_{VS}\right)^2\left(\Delta_L - \Delta_S\right)^2\right) + \\ \left(e_S e_M\right)^2\left(\Delta_L - \Delta_{VS}\right)^2 + \left(e_S e_L\right)^2\left(\Delta_M - \Delta_{VS}\right)^2 + \\ \left(e_S e_M\right)^2\left(\Delta_L - \Delta_{VS}\right)^2 + \left(e_L e_M\right)^2\left(\Delta_{VS} - \Delta_S\right)^2\end{array}\right)}{\left(e_S e_M e_L\right)^2 + \left(e_{VS} e_M e_L\right)^2 + \left(e_{VS} e_S e_L\right)^2 + \left(e_{VS} e_S e_M\right)^2} \quad (3)$$

For bright illumination levels, receptor noise is assumed to be a constant determined only by the Weber fraction, w_f and the relative population density, g_r, for each r[th] cone class (Renoult et al., 2015): $e_r = w_f \Big/ \sqrt{g_r}$. For peafowl, we used the value for chromatic Weber fractions of $w_f =$ 0.06 for L cones for domestic chickens based on color discrimination (Olsson et al., 2015). Receptor noise values for the other single cone classes were estimated using mean peafowl relative population densities $g_r = (0.477, 0.892, 1.047, 1)$ for (VS, SWS, MWS, LWS) (Hart, 2001), yielding $e_r = (0.087, 0.064, 0.06, 0.06)$. For parrots, we used $g_r = 0.25{:}0.33{:}1.05{:}1$ and w_f = 0.105 found for spectral sensitivity in *Melopsittacus undulatus* (Lind et al., 2014),

corresponding to e_r = (0.210, 0.182, 0.102, 0.105). Because color discrimination has not been measured for other mammals (Olsson et al., 2017), following (Stoddard et al., 2019) we used w_f = 0.22 found for brightness discrimination in domestic dogs (range 0.22-0.27) (Pretterer et al., 2004). The relative cone population fractional densities measured for domestic cats (Linberg et al., 2001) give a mean g_r(S,L) = (0.12,1); similar ratios have been reported for various wild felids (Ahnelt et al., 2006) and domestic dogs (Mowat et al., 2008). This gives the estimated predator receptor noise for color discrimination as (e_S, e_L) = (0.64, 0.22).

The brightness contrast, ΔS_L, between each pqth pair of color patches was computed from the quantum catches, Q_{Lp} for the pth color patch for the spectral response for the luminance channel (double cones for birds and L cones for dichromat predators) using $\Delta S_L = (\log Q_{Lp} - \log Q_{Lq})/w_f$, where w_f is the Weber fraction for brightness discrimination. For birds, we used w_f = 0.18 measured for double cones in budgerigars (*Melopsittacus undulatus*) (Lind et al., 2013); for comparison, lower values 0.10 have been found for pigeons (Hodos et al., 1985) and higher values $\geq$ 0.24 for chicks of the domestic chicken (Jones and Osorio, 2004). For predators, we used w_f = 0.22 for brightness discrimination in domestic dogs as explained above; for comparison, w_f = 0.10 in humans, and $w_f \leq$ 0.45 in other mammals (Maertens and Wichmann, 2013; Olsson et al., 2017).

Color and brightness contrasts are interpreted in units of just noticeable distances (JND), with JND = 1 corresponding to the threshold for two patches to be discriminable under ideal illumination and viewing conditions when suitable data exist for the visual system being modeled (Olsson et al., 2015; Vorobyev and Osorio, 1998). Behavioral studies have shown that

birds detect colorful fruit at a rate that correlates with increasing color (but not brightness) contrast for values >> 1 JND (Cazetta et al., 2009), while in lizards, the probability of discriminating a color from its background was found to be < 20% at 1 JND and to scale approximately linearly over the range $1 \leq JND \leq 12$ (Fleishman et al., 2016). Behavioral tests in zebra finches have found that color contrast detection thresholds range from JND = 1 to 2.5 to 3.2, depending on background color (Lind, 2016). Following (Siddiqi et al., 2004), we therefore assume that the contrast detection threshold is approximately JND = 1 and we define contrasts in the range $1 < JND \leq 3$ as weakly detectable.

Pattern Analysis

To model the perception of visual texture of the peacock's train viewed against foliage, we also performed granularity pattern analysis on the model peacock train photographs, using MATLAB code adapted from (Barbosa et al., 2008) and MICA's granularity texture analysis package. In granularity analysis, an image based on the luminance channel is filtered using an FFT bandpass filter centered at a series of spatial frequencies (granularity bands). For each bandpass-filtered image, the "pattern energy" (a measure of information at each spatial scale) is computed as the standard deviation of its pixel intensity values. The "granularity spectrum" then is defined as pattern energy vs granularity band. Granularity analysis was performed on the model peacock train images processed for the dichromatic predator luminance channel as explained above. Granularity spectra were computed for polygonal regions of interest (ROI) encompassing the entire model train and each type of surrounding vegetation (i.e., tall grass, brush or trees). To compensate for the effect of ROI shape and background, we used the following method adapted from MICA. For each ROI, we first computed a masked image in which all regions outside the

ROI were replaced by a black background. Next, we created a mean masked image in which the region inside the ROI in the masked image was replaced by the mean intensity within the ROI. Identical granularity calculations were performed on both images and their difference was used to create a shape-independent granularity spectrum.

We also computed summary statistics for comparing textures of the model train and its background: total energy (the energy summed across all filter bands, which increases as pattern contrast increases), peak filter size (the granularity band at peak energy; larger peak filter size corresponds to smaller most prevalent feature size), and proportion energy (the maximum energy divided by the total energy, a measure of how much of the spectral energy lies at the most prevalent feature size; this decreases with increasing pattern scale diversity). Granularity spectrum were plotted as "normalized energy" (pattern energy divided by total energy) vs granularity band to give a measure of how pattern information is distributed across spatial scales. Images with a uniform distribution of pattern scales have correspondingly uniform granularity spectra, while images dominated by a single feature scale should have strongly peaked spectra.

Edge detection of the luminance channel image provides an alternative measure of pattern complexity. We used the Canny edge filter in MATLAB to find edges using sigma = 3 and threshold = 0.15 to 0.20 (relative to maximum luminance image intensity set to 1) (Lovell et al., 2013; Melin et al., 2016). Model train images were first log transformed and then processed using contrast-limited adaptive histogram equalization (Zuiderveld, 1994) (*adapthisteq* in MATLAB) to detect texture edges in regions of widely differing illumination. The edge fraction (percentage of edge pixels in each ROI) was then used to compare the model train with various

454 types of vegetation in the background (Stoddard et al., 2016); higher edge fractions indicate a
455 more complex pattern with more spatial features.
456

457 Statistics

458 Our analysis of color and brightness contrasts followed the two-step process recommended in
459 (Maia and White, 2018). First, to determine whether the mean color and brightness contrasts
460 between each patch pair had a statistically significant difference given their variances, we used
461 PERMANOVA modified for non-normal, heterogeneous data (Anderson et al., 2017)
462 implemented in the software package FATHOM (Jones, 2017) using 1000 bootstrap samples.
463 Note that is it possible for this difference to be statistically significant, but to have value too
464 small for it to be perceptually distinguishable. We therefore determined the effect size (how
465 perceptually distinct each color patch pair) as follows. We first drew with replacement 1000
466 bootstrapped sample pairs using the MATLAB command *datasample*, and computed the mean Δ
467 S_C and ΔS_L for this bootstrap resample. These mean contrasts were averaged over all images to
468 get the mean and s.e.m. for each color patch pair for each sample; the grand mean and s.e.m. then
469 was computed by averaging over all replicates for each feather type. Grand means and s.e.m. for
470 the texture summary statistics were calculated from the mean of each statistic taken over all
471 model train data for the train, grass, brush, and tree foliage. All results are reported as grand
472 mean [95% CI = 2 s.e.m].
473

474 Data Accessibility

475 All data and software required in order to replicate all of our results are archived either in the
476 supplemental materials or at https://figshare.com/s/f8add694af9c79de7f76.

Results

Reflectance spectroscopy

Reflectance spectra for peacock eyespot feather color patches (Fig 2D) and peacock iridescent blue plumage (Fig. 2E) had spectral peaks consistent across repeated measured to 4 to 16 nm (95% CI) and exhibited similar spectral peaks and overall shape to those measured for zero elevation angle (Dakin and Montgomerie, 2013; Loyau et al., 2007; Yoshioka and Kinoshita, 2002). A comparison of cone spectral sensitivity data (Fig 2C) with these reflectance spectra show that the peacock SWS cone is well matched to reflectance from its iridescent peacock blue plumage. While the spectral peaks for the bronze (BZ), blue-green (BG) and outer loose green (GB) barbs agree well with its SWS, MWS and LWS cone spectral ranges, all three also coincide with the same L cone sensitivity for the predator. Both the predator and peafowl VS cone spectral sensitivities also overlap with the reflectance spectrum from the eyespot's central BB and PB dark violet patches. However, reflectance from these features is weak compared to the other color patches, all of which also reflect weakly in the UV. Fig 2E shows the reflectance spectrum of a representative green leaf, illustrating how its peak at approximately 550 nm and its overall spectra resemble that of the peacock's loose green barbs; similar spectra for green background foliage have been reported in (Cazetta, Schaefer, and Galetti 2009; Loyau et al. 2007).

Reflectance spectra for parrot feathers (Fig 3E) agreed with previously published values (Tinbergen et al., 2013), confirming a good spectral match between yellow and red feather

reflectance with MWS and LWS avian cone sensitivities. The predator L cone sensitivity spans a spectral range corresponding to longer wavelength reflection from both yellow and red pigments (Fig. 3D). Both the yellow and red patches also have reflectance peaks in the UV with a better overlap with bird UVS cone sensitivity than that of VS cones.

A comparison of the peak spectral sensitivities of S and L cones for canids, domestic cats and ferrets with those for the four single cone populations of 21 bird species from 8 different orders (Hart and Hunt, 2007) (Fig 5) illustrates that predator S cones have a peak response similar to that of bird VS, but not UVS, cones. The predator S peak values lie between most peaks of the avian UVS/VS and SWS cone populations, whereas predator M peak values lie between avian MWS and LWS peak values.

Fig 5. Comparison of peak spectral responses of predator and bird cones. Peak single cone spectral sensitivities for ferret S and L cones (Douglas & Jeffery, 2014) and for bird VS/UVS, SWS,MWS and LWS cones from Fig 5B in (Hart & Hunt, 2007) for 21 species of birds from 9 orders.

Color and brightness contrast analysis

False color images and analyses using the receptor noise model of visual discrimination are shown in Fig 6-9; all data and PERMANOVA pseudo-F and P values are reported in S1-S4 Datasets. Note that these false color images should be considered as a relative guide and not an

absolute indication of the detectability of contrasts because humans have better contrast thresholds than dichromatic mammals by a factor of 3.7 for color and 2 for brightness, as well as similar color contrast thresholds and better brightness thresholds by a factor of ≥ 1.6 for birds (Olsson et al., 2015, 2017). To provide context for the measured color and brightness contrasts between feathers and green saucer magnolia leaves, we also found that the contrasts between leaves from the saucer magnolia and seven other plant species with different shades of green were statistically significant (with one exception out of 27 pairs) with tetrachromatic bird vision $\Delta S_C = 2.75$ [2.23, 3.28] and $\Delta S_L = 3.30$ [2.64, 3.97] and dichromatic mammal vision $\Delta S_C = 0.55$ [0.42, 0.69] and $\Delta S_L = 2.53$ [2.01, 3.06] (mean [95% CI]) (S3 Fig).

Fig 6. False color images and color and brightness contrast analysis of peacock eyespot feathers. (A) False color images modelling peafowl and dichromatic mammalian predator vision of peafowl eyespot and green leaf (inset at bottom of eyespot image) for different viewing distances. Note that the false color images should be considered as a relative guide and not an absolute indication of the detectability of contrasts because humans have better contrast thresholds by a factor of 3.7 for color and 2 for brightness compared to dichromatic mammals. (B)-(E) Estimated color (delta S_C) and brightness (delta S_L) contrasts for adjacent color patches on the peacock eyespots and green vegetation, over a range of viewing distances. All data are shown as grand means with 95% CI error bars. Contrasts corresponding to the same distance have been displaced by horizontal jitter to avoid overlap. Data above the 1 JND line are above the expected threshold for discrimination and contrasts within the grey shaded regions are at most weakly detectable. Closed symbols indicate contrasts that are statistically significant in each organism's colorspace (i.e., PERMANOVA $P < 0.05$); note that contrasts that are not

544 statistically significant (closed symbols) due to their large, overlapping variances in the
545 corresponding colorspace may still have mean values greater than the detection threshold.
546
547 **Fig 7. False color images and color and brightness contrast analysis of the peacock model**
548 **train photographed against various types of vegetation backgrounds.** (A) False color images
549 in peafowl and dichromatic mammalian predator vision of peafowl model train for different
550 viewing distances. (B)-(E) Color and luminance contrasts for the model train and features of
551 vegetation, over a range of viewing distances. All data are shown as grand means with 95% CI
552 error bars. See Fig 6 caption for further details.
553
554 **Fig 8. False color images and color and brightness contrast analysis of peacock blue neck**
555 **feathers used to model the body's appearance against green foliage.** (A) False color images
556 in peafowl and dichromatic mammalian predator vision of peacock blue breast plumage vs green
557 foliage for different viewing distances. (B)-(E) Color and luminance contrasts for the blue
558 plumage relative to green vegetation, over a range of viewing distances. See Fig 6 caption for
559 further details.
560
561 **Fig 9. False color images and color and brightness contrast analysis of parrot feathers.** (A)
562 False color images in parrot ultraviolet sensitive (UVS) and dichromatic mammalian predator
563 vision of scarlet macaw, African grey parrot and Amazon parrot red and yellow feathers vs green
564 leaf for different viewing distances. (B)-(E) Color and luminance contrasts for parrot feather
565 colors relative to green vegetation, over a range of viewing distances. See Fig 6 caption for
566 further details.

False color images for various simulated viewing distances are displayed for peacock eyespot feathers in Fig 6A and visual signals are plotted vs distance in Fig 6B-E. In peafowl vision, all pairs of adjacent color patches in the peacock's eyespot give large, statistically significant color contrasts > 3 JND for all distances. The greatest color contrasts were between the blue-green patch and surrounding rings and between the two central pupil-like patches; for some distances ≤ 8 m these same pairs of color patches also had statistically significant brightness contrasts in the 1-3 JND low detectability range. By contrast, in dichromat vision none of the eyespot patch pairs had color contrasts above 1 JND, and only the three innermost pairs of eyespot patches had brightness contrasts that were in the weakly detectable 1-3 JND range.

For peafowl vision, at all distances the model peacock train had statistically significant color and brightness contrasts that were > 3 JND for brush and trees, but not grass (Fig 7; additional false color images in S4 Fig). In dichromat predator vision, all color contrasts for the model train were < 1 JND and brightness contrasts were in the weakly detectable 1-3 JND range. Peacock blue plumage was found to be perceptually detectable by conspecifics at all distances and to lie in the weakly detectable 1-3 JND range for dichromat vision (Fig 8). The false color images of peacock feathers (Fig 6, 7, 8, S4 Fig) demonstrate how color signals relative to background vegetation are diminished when the single dichromat L cone replaces the separate SWS/MWS/LWS cones for birds, especially at larger distances.

Red and yellow parrot feather color patches exhibited large, statistically significant contrasts in avian UVS vision in general, with color contrasts > 3 JND for ≤ 8 m and brightness contrasts > 1

JND for most samples (Fig 9) By contrast, for dichromat vision, none of the red parrot patches and the African grey parrot and scarlet macaw yellow patches had color contrasts > 1 JND, and the Amazon parrot feather yellow patches just exceeded 1 JND for ≤ 4 m. For distances ≤ 8 m, red parrot feather patches had brightness contrasts in the weakly detectable 1-3 JND range for ≤ 8 m and yellow patches had mean values in the range 2.4-6.7 JND.

Pattern analysis

Fig 10 and S4 Fig show false color images and granularity spectra for the peacock's train and different types of background vegetation (tall grass, brush and trees) for the various viewing distances modeled (S5 Dataset). Because the spatial frequency of objects in an image as well as an animal's visual field depend on distance, we would expect objects with similar textures observed at different distances to have similarly-shaped spectra, but possibly different frequency peaks and widths. Granularity spectra for the peacock's train (Fig. 10B) indeed had the same shape as those for background vegetation in that each had a single broad peak for granularity band values > 3. The peak spatial frequencies of each granularity spectrum moved to lower values as viewing distance increased, as expected from the blurring of fine scale features. For all distances, the peacock's train and background vegetation had values of proportion energy, peak frequency and total energy that agreed at the 95% CI, with the only exception that the proportion energy for distances > 4 m differed between the model train and trees (Fig. 9D-F). Collectively, these results demonstrate that the peacock's erect train is an excellent match for the predominant feature size distribution, overall contrast and pattern scale diversity of background vegetation. Moreover, visual examination of the edge detected images (Fig 10A, S5 Fig) suggests that the

612 calculated edge fractions for the train and background foliage agreed at the 95% CI level at all
613 distances (Fig 9G).
614
615 **Fig 10. Texture analysis of the model peacock train photographed against various**
616 **vegetation backgrounds.** (A) Image based on dichromatic mammalian predator luminance
617 channel and (B) result of edge detection on the luminance image. (C) Granularity spectrum for
618 the model peacock train and three different regions of vegetation in the background vs viewing
619 distance. (D) Total spectral energy summed over the granularity spectrum, which gives a
620 measure of overall pattern contrast. (E) Proportional energy, a measure of how much the
621 dominant feature size dominates and hence pattern diversity; (F) spatial frequency at peak
622 spectral energy, which is inversely proportional to the predominant feature size; (G) edge
623 fraction, the proportion of the image corresponding to edges. Data are grand means for all model
624 train images and error bars show 95% CI.
625

626 Discussion

627 The results of our study show that sexually-selected color signals readily detectable by
628 conspecifics are not necessarily conspicuous to mammalian predators. Instead, for all distances
629 considered, the color and brightness contrasts for all feather samples studied here relative to
630 green foliage were much greater for birds than for dichromatic mammals. For viewing distances
631 of 1 m and more, most feather samples (peacock eyespot, model peacock train and red feathers,
632 and all yellow feathers but those of the scarlet macaw at $\leq$ 2 m) had color contrasts in
633 dichromatic vision that were perceptually indistinguishable from background vegetation at all
634 distances considered here. Unsurprisingly, the same feathers were highly conspicuous to

conspecifics: their color contrasts were comparable to values found for avian visual modeling for fruit viewed against green foliage (Cazetta et al., 2009; Fadzly et al., 2013). The brightness contrasts for these feathers vs background foliage in dichromatic predator vision were on the whole greater than the corresponding color signals, although only values for yellow exceeded the weakly detectable 1-3 JND range. This suggests that patterns with high brightness contrast, such as those created by white and dark melanin-pigmented plumage, might be more readily detectable by dichromat predators than color signals, and thus represent a greater detection risk (Montgomerie et al., 2001). While the interpretation of supra-threshold color and brightness contrasts is still debated (Stuart-Fox, 2018), our results show that such supranormal stimuli remain detectable by conspecifics and other birds even at large distances where carnivores cannot perceive them.

Considering parrot feathers in particular, we note that red plumage is at best weakly detectable given its sub-threshold color contrasts and low brightness contrasts when viewed by dichromatic mammals against green foliage, although yellow parrot feathers have brightness contrasts that should be more readily detectable by mammalian predators at close distances. A consideration of cone spectral sensitivities and feather reflectance spectra suggest two reasons for this difference. First, these yellow feathers had an overall higher reflectance than the corresponding red feathers, resulting in their having a higher brightness contrast relative to leaves. Second, yellow feather pigments reflect considerable light in the UV compared to red pigments, whereas UV reflectance is low for green plants. Yellow feathers thus stimulate both predator S and L cones, while green plants primarily stimulate the L cones, providing a mechanism for distinguishing yellow feathers from green foliage backgrounds.

These conclusions should hold for other birds with red and yellow plumage given that a wide variety of species of birds have similar color vision to the species considered here (Fig 5), and that feathers colored with carotenoid pigments have very similar reflectance spectra to the pigment psittacofulvin found in parrot feathers (Shawkey and Hill, 2005; Toral et al., 2008). Thus, our findings indicate that many species of red and yellow feathered birds that appear conspicuous to other birds and humans may in fact be cryptic or poorly visible to predators because of background matching (Stevens and Merilaita, 2011). Our findings also have broader implications for interpreting how color cues, camouflage and possible eye mimicry appear to the majority of mammals. Trichromacy in primates has been suggested to have evolved for a variety of reasons (Carvalho et al., 2017), including detecting ripe fruit and immature leaves, breaking camouflage (e.g., during foraging for eggs) (Troscianko et al., 2017), sexual or social signaling (Hiramatsu et al., 2017), and predator detection (Pessoa et al., 2014). Our results suggest that the evolution of trichromacy may also have provided catarryne primates, howler monkeys and some marsupials with an advantage in detecting colorful birds, reptiles, amphibians and insects.

Ultraviolet vision per se does not result in these differing visual signals: these dichromatic mammalian predators have similar near-UV S cone spectral sensitivity to the VS cones of birds (Douglas and Jeffery, 2014; Stevens and Cuthill, 2007). Indeed, as noted above, since red and yellow parrot feathers and the central patches on peacock feathers reflect appreciable UV light this may make these feathers more detectable by dichromats. It is therefore important to include UV reflectance in modeling of visual signals in dichromatic mammalian visual systems, as opposed to relying on image processing of human visible RGB photographs (Pongrácz et al.

2017). These results also are not merely a consequence of birds having more types of cones than carnivores: given the similar spectral response of dichromatic mammal S and L cones and avian VS and MWS cones, color patches could in principle generate similar contrasts in both visual systems. Instead, these feathers have low contrast in dichromatic mammal vision due to a combination of low visual acuity, higher receptor noise levels and poorer spectral discrimination over the L cone response range.

Focusing now on peacock eyespots, the large color contrasts for peafowl vision arise from spectral tuning between the reflectance spectra of each peacock eyespot color patch and peafowl single cone spectral sensitivities, similar to the agreement reported earlier between red and yellow pigment reflectance spectra and tetrachromatic UVS cone responses for parrot plumage and vision (Tinbergen et al., 2013). It is especially notable that the greatest color contrasts are due to the blue-green ring, since its iridescence has been found to correlate with peacock mating success (Dakin and Montgomerie, 2013; Loyau et al., 2007), and its chromatic contrast was calculated to be the most salient signal in images of a displaying peacock (Pike, 2018).

When we computed measures for the model peacock train against a foliage background in dichromatic predator vision, the train feathers were found to have below detection threshold color contrasts and brightness contrasts in the low detectability 1-3 JND range, similar in magnitude to those for various types of green vegetation. Taken together with the eyespot and textural analysis results, this indicates that dichromatic mammalian predators are likely unable to discriminate the peacock's train from green vegetation during foraging, although the eyespot's innermost features create low detectable brightness contrasts at nearby distances. Contrary to

common assumption, this suggests the counterintuitive hypothesis that that both the color and brightness contrasts might function as disruptive camouflage for peacocks viewed from a distance, making the train difficult to distinguish as a whole (Hillgarth, 1984; Ridley et al., 1984; Stevens and Merilaita, 2011).

The peacock's blue plumage had large, detectable levels of color contrast at all distances for peafowl vision, though both color and brightness contrasts were in the low detectable range for dichromatic predator vision. Thus, the blue head, neck and breast contour feathers may represent a greater visual signal for distant conspecifics, as well as a greater predation risk, than the much larger train; however, all of these values are likely less conspicuous when forest shade diminishes their blue hue. Given that noniridescent blue feathers from other birds have been shown to have similar reflectance spectra to peafowl blue plumage, these results are likely generalizable (Osorio and Ham, 2002).

Do peacock eyespots mimic eyes in appearance when viewed by conspecifics or by predators? Eyes and eye-like patterns have been shown to be highly salient visual signals for birds, humans and domestic dogs (Somppi et al., 2016; Stevens and Ruxton, 2014; Yorzinski et al., 2015). However, our false color images show that peafowl eyespots do not always appear to have a central dark, circular pupil when viewed at typical display distances, either in peafowl or dichromatic mammalian predator visual models (Fig 11A,B,C). Therefore, it is not obvious that peacock ocelli appear eye-like to nearby viewers. On the other hand, blurring at larger distances $\leq$ 8 m causes eyespots to appear to have pupil-like dark centers in dichromatic predator vision,

indicating that they may indeed appear eyelike to predators when viewed at this intermediate range (Fig 11D).

Fig. 11. False color images of peacock eyespots show that eye-mimicry depends on viewing distance. At 1 m, peacock eyespots have central features with brightness comparable to the surrounding rings in false color images for peafowl vision in the (A) LWS/MWS/SWS and (B) VS cone channels, and for dichromatic mammals (C). False color image of the model train in dichromatic mammalian vision at 2 meters (D) show that the eyespots feature a darker pupil-like center at distances ≤ 8 m.

Taken as a whole, these results call into question the widely-held assumption that the peacock's eyespot feathers are highly conspicuous for all viewers. Indeed, (Hillgarth, 1984) noted that even to humans the peacock's train can be well camouflaged against foliage in its native habitats and (Ridley et al., 1984) has suggested that peafowl eyespots originated as a form of camouflage for their native dappled light environments. Motion cues during peafowl displays and other behaviors might enhance the detectability of their visual signals, although evidence is mixed whether motion increases or decreases visual contrast thresholds (Hodos et al., 2003). On the other hand, the motions of the flexible loose green barbs in the train might also simulate that of background brush and grasses, a visual illusion studied in insects, crabs, spiders and lizards but not yet in birds (Peters et al., 2008). Future video studies could utilize cameras adapted for multispectral imaging provided with a filter that transmits light from the near-UV to 700 nm.

748 Supporting these conclusions, we have been unable to find any data in the literature supporting
749 the idea that the peacock with trains experience a significant, let alone an enhanced, risk of
750 predation compared to, e.g., either peacocks without trains or peahens. In fact, one survey of a
751 feral peafowl population (Petrie, 1992) found that predated adult peacocks tended to have
752 relatively small trains and lower mating success. Another study found that peafowl are preyed
753 on far less by leopards than expected given that they were the most abundant prey species in the
754 region studied (Mondal et al., 2011). Adult peacocks are reported to have several effective anti-
755 predator strategies, including running (Ali and Ripley, 1981; Thavarajah et al., 2016; Wilkinson
756 et al., 2015), flight (Askew, 2014), fighting with their sharp spurs (Petrie et al., 1991), hiding in
757 dense thickets (Ali and Ripley, 1981; Harikrishnan et al., 2010; de Silva et al., 1996), and using
758 group vigilance along with alarm calling (Yasmin and Yahya, 2000). At dusk, they roost in high
759 trees chosen for their protection against predators (de Silva et al., 1996; Trivedi and Johnsingh,
760 1996). As a result, peafowl appear to be at highest risk of predation primarily during their first
761 year (de Silva et al., 1996).
762
763 The available evidence thus indicates that any putative enhanced risk of predation or other
764 handicap suffered by adult peacocks is likely to be incurred by factors other than visual signals
765 created by their eyespot train feathers. For example, peacocks spend a large percentage of their
766 time maintaining their plumage (Walther, 2003) and displaying (Dakin and Montgomerie, 2009;
767 Harikrishnan et al., 2010). Thus, the elaborate courtship displays of peacocks may correspond to
768 handicaps due to the conspicuous appearance of their blue plumage, time lost from foraging for
769 food due to plumage maintenance and courtship displays, the male's likely inattention to

predators during displays, and the metabolic demands of the male's courtship displays (Vehrencamp et al., 1989).

It is important to note that several other factors may result in feathers having even lower visual contrasts in predator vision than reported here. First, our viewing and illumination geometries were chosen to optimize color and brightness cues. Second, when feathers are viewed at low illumination levels either in dim forest lighting or at twilight or night, they also are likely to have lower color and brightness contrasts (Freitag and Pessoa, 2012; Sicsú et al., 2013). Furthermore, since UV reflectance helps distinguish feathers from green foliage, the reduction in UV irradiance in forest shade is likely to render feathers less detectable in forest shade than in direct sunlight (Endler, 1993). Third, we also modeled only distance-dependent blurring due to visual acuity (retinal sampling), but a more complete treatment would use each species' behaviorally measured contrast sensitivity function (CSF) (Melin et al., 2016) to account for the optics of the eye and other factors that have determined for our study species (Jarvis and Wathes, 2007). While we lacked the data to perform this additional analysis, the additional blurring would make dichromatic predators even less likely to be able to detect the feathers than our estimated contrasts indicate. Fourth, we chose to compare feathers with relatively dark green leaves (S3 Fig). The small variation in color contrasts indicates our findings are generalizable to other shades of green, while suggesting that feathers should be even less visible against light green foliage. Thus, our results likely overestimate the detectability of these feathers by dichromatic mammals.

The largest source of uncertainty in our analysis is the lack of behaviorally-measured Weber fractions for color contrast for terrestrial carnivorans for the conditions considered here. This data also would be valuable for studies that often have had to rely on human visual modeling in analyzing egg camouflage (Stoddard et al., 2016) and the relationship between plumage, brightness and antipredator vigilance (Pascual et al., 2014). The most relevant measures would involve behavioral tests to determine whether these mammals can detect feathered model birds when other cues (e.g., olfactory) are controlled for. Any such studies ought to be sure to use illumination sources that include UV, as well as color cues that closely match the reflectance spectra of natural objects (Stoddard et al., 2019).

Darwin stated that "Even the bright colors of many male birds cannot fail to make them conspicuous to their enemies of all kinds" (Darwin, 1888). On the contrary, our study implies that some species of birds that appear vividly colorful to humans and other birds may appear drab and inconspicuous in the eyes of mammalian predators. This conclusion is consistent with the finding that susceptibility to cat predation does not correlate significantly with sexual dichromatism in birds (Møller et al., 2010). The predation risk incurred by colorful plumage instead depends on specifics of pigmentation, photoreceptor response, and environmental context, as suggested by sensory drive theory (Cummings and Endler, 2018), and thus should be assessed on a case-by-case basis.

Predators have a variety of other means of detecting prey, including visual motion perception and sensing acoustic, tactile and olfactory cues. Our results highlight the importance of understanding how dynamic behaviors during multimodal displays, foraging and other activities

make birds more apparent to mammals and other predators than do their seemingly-conspicuous colors alone.

Acknowledgements

We wish to thank Cassie Stoddard for providing us with her edge detection code, Charles Chubb and Roger Hanlon for their granularity code, and Robert Beyer for instrumentation design.

Financial Disclosure

Haverford College awards to Suzanne Amador Kane, Rui Fang, and Yabin Lu, and Yuchao Wang, www.haverford.edu; Natural Sciences and Engineering Research Council of Canada (NSERC), Postdoctoral Fellowship to Roslyn Dakin www.nserc-crsng.gc.ca

Competing Interests

The authors have declared that no competing interests exist.

Author contributions

Conceptualization: S.A.K., R.D.; Methodology: S.A.K., R.F., Y.L., Y.W; Investigation: S.A.K, R.F., Y.L., Y.W; Data curation: S.A.K., Y.W.; Software: S.A.K., Y.W.; Validation: S.A.K., Y.W.; Visualization: S.A.K., R.F., Y.L., Y.W; Formal analysis: S.A.K.,.W.; Writing – original draft: S.A.K.; Writing – review & editing: S.A.K., R.D., R.F., Y.L., Y.W.

References

Ahnelt, P.K., Schubert, C., Kübber-Heiss, A., Schiviz, A., and Anger, E. (2006). Independent variation of retinal S and M cone photoreceptor topographies: A survey of four families of mammals. Visual Neuroscience *23*, 429–435.

Akkaynak, D., Siemann, L.A., Barbosa, A., and Mäthger, L.M. (2017). Changeable camouflage: how well can flounder resemble the colour and spatial scale of substrates in their natural habitats? Royal Society Open Science *4*, 160824.

Ali, S., and Ripley, S.D. (1981). Handbook of the Birds of India and Pakistan: Together with Those of Bangladesh, Nepal, Bhutan and Sri Lanka Volume 2: Megapodes to Crab Plover (Oxford University Press).

Anderson, M.J., Walsh, D.C.I., Clarke, K.R., Gorley, R.N., and Guerra-Castro, E. (2017). Some solutions to the multivariate Behrens–Fisher problem for dissimilarity-based analyses. Australian & New Zealand Journal of Statistics *59*, 57–79.

Askew, G.N. (2014). The elaborate plumage in peacocks is not such a drag. Journal of Experimental Biology *217*, 3237–3241.

Barbosa, A., Mäthger, L.M., Buresch, K.C., Kelly, J., Chubb, C., Chiao, C.-C., and Hanlon, R.T. (2008). Cuttlefish camouflage: The effects of substrate contrast and size in evoking uniform, mottle or disruptive body patterns. Vision Research *48*, 1242–1253.

Barnett, J.B., Michalis, C., Scott-Samuel, N.E., and Cuthill, I.C. (2018). Distance-dependent defensive coloration in the poison frog Dendrobates tinctorius, Dendrobatidae. PNAS *115*, 6416–6421.

Barreira, A.S., García, N.C., Lougheed, S.C., and Tubaro, P.L. (2016). Viewing geometry affects sexual dichromatism and conspicuousness of noniridescent plumage of Swallow Tanagers (Tersina viridis). The Auk *133*, 530–543.

Beebe, W. (1918). A Monograph of the Pheasants (Witherby & Co).

Calderone, J.B., and Jacobs, G.H. (2003). Spectral properties and retinal distribution of ferret cones. Visual Neuroscience *20*, 11–17.

Carvalho, L.S., Pessoa, D.M.A., Mountford, J.K., Davies, W.I.L., and Hunt, D.M. (2017). The Genetic and Evolutionary Drives behind Primate Color Vision. Front. Ecol. Evol. *5*.

Caves, E.M., and Johnsen, S. (2018). AcuityView: An r package for portraying the effects of visual acuity on scenes observed by an animal. Methods in Ecology and Evolution *9*, 793–797.

Cazetta, E., Schaefer, H.M., and Galetti, M. (2009). Why are fruits colorful? The relative importance of achromatic and chromatic contrasts for detection by birds. Evol Ecol *23*, 233–244.

Chiao, C.-C., Wickiser, J.K., Allen, J.J., Genter, B., and Hanlon, R.T. (2011). Hyperspectral imaging of cuttlefish camouflage indicates good color match in the eyes of fish predators. PNAS *108*, 9148–9153.

870 Clark, D.L., and Clark, R.A. (2016). Neutral point testing of color vision in the domestic cat.
871 Experimental Eye Research *153*, 23–26.

872 Cronin, T.W., Johnsen, S., Marshall, N.J., and Warrant, E.J. (2014). Visual Ecology (Princeton
873 University Press).

874 Cummings, M.E., and Endler, J.A. (2018). 25 Years of sensory drive: the evidence and its
875 watery bias. Curr Zool *64*, 471–484.

876 Dakin, R., and Montgomerie, R. (2009). Peacocks orient their courtship displays towards the
877 sun. Behav Ecol Sociobiol *63*, 825–834.

878 Dakin, R., and Montgomerie, R. (2013). Eye for an eyespot: how iridescent plumage ocelli
879 influence peacock mating success. Behav Ecol *24*, 1048–1057.

880 Dakin, R., McCrossan, O., Hare, J.F., Montgomerie, R., and Kane, S.A. (2016). Biomechanics
881 of the peacock's display: How feather structure and resonance influence multimodal signaling.
882 PLOS ONE *11*, e0152759.

883 Dalrymple, R.L., Hui, F.K.C., Flores-Moreno, H., Kemp, D.J., and Moles, A.T. (2015). Roses are
884 red, violets are blue – so how much replication should you do? An assessment of variation in
885 the colour of flowers and birds. Biol J Linn Soc *114*, 69–81.

886 Darwin, C. (1888). The descent of man and selection in relation to sex (Murray).

887 Douglas, R.H., and Jeffery, G. (2014). The spectral transmission of ocular media suggests
888 ultraviolet sensitivity is widespread among mammals. Proceedings of the Royal Society of
889 London B: Biological Sciences *281*, 20132995.

890 Endler, J.A. (1980). Natural Selection on Color Patterns in Poecilia Reticulata. Evolution *34*, 76–
891 91.

892 Endler, J.A. (1991). Interactions between predator and prey. Behavioural Ecology 169–202.

893 Endler, J.A. (1993). The Color of Light in Forests and Its Implications. Ecological Monographs
894 *63*, 1–27.

895 Endler, J.A. (2012). A framework for analysing colour pattern geometry: adjacent colours. Biol J
896 Linn Soc *107*, 233–253.

897 Fadzly, N., Burns, K.C., and Zuharah, W.F. (2013). Evaluating Frugivore-fruit Interactions Using
898 Avian Eye Modelling. Trop Life Sci Res *24*, 31–50.

899 Fleishman, L.J., Perez, C.W., Yeo, A.I., Cummings, K.J., Dick, S., and Almonte, E. (2016).
900 Perceptual distance between colored stimuli in the lizard Anolis sagrei: comparing visual system
901 models to empirical results. Behav Ecol Sociobiol *70*, 541–555.

902 Freeman, A.R., and Hare, J.F. (2015). Infrasound in mating displays: a peacock's tale. Animal
903 Behaviour *102*, 241–250.

904 Freitag, F.B., and Pessoa, D.M.A. (2012). Effect of luminosity on color discrimination of
905 dichromatic marmosets (Callithrix jacchus). J. Opt. Soc. Am. A, JOSAA *29*, A216–A222.

Gokula, V. (2015). Display behaviour of Indian Peafowl Pavo cristatus (Aves: Galliformes) during the mating season in viralimalai, TamilNadu, India. TAPROBANICA: The Journal of Asian Biodiversity *7*.

Guenther, E., and Zrenner, E. (1993). The spectral sensitivity of dark- and light-adapted cat retinal ganglion cells. J. Neurosci. *13*, 1543–1550.

Harikrishnan, S., Vasudevan, K., and Sivakumar, K. (2010). Behavior of Indian peafowl Pavo cristatus Linn. 1758 during the mating period in a natural population. The Open Ornithology Journal *3*, 13–19.

Hart, N.S. (2001). Variations in cone photoreceptor abundance and the visual ecology of birds. J Comp Physiol A *187*, 685–697.

Hart, N.S. (2002). Vision in the peafowl (Aves: Pavo cristatus). Journal of Experimental Biology *205*, 3925–3935.

Hart, N., and Hunt, D. (2007). Avian visual pigments: characteristics, spectral tuning, and evolution. The American Naturalist *169*, S7-26.

Hart, N.S., Partridge, J.C., Cuthill, I.C., and Bennett, A.T.D. (2000). Visual pigments, oil droplets, ocular media and cone photoreceptor distribution in two species of passerine bird: the blue tit (Parus caeruleus L.) and the blackbird (Turdus merula L.). J Comp Physiol A *186*, 375–387.

Håstad, O., Victorsson, J., and Ödeen, A. (2005). Differences in color vision make passerines less conspicuous in the eyes of their predators. PNAS *102*, 6391–6394.

Hillgarth, N. (1984). Social organization of wild peafowl in India. World Pheasant Assoc J *9*, 47–56.

Hiramatsu, C., Melin, A.D., Allen, W.L., Dubuc, C., and Higham, J.P. (2017). Experimental evidence that primate trichromacy is well suited for detecting primate social colour signals. Proc. R. Soc. B *284*, 20162458.

Hodos, W., Bessette, B.B., Macko, K.A., and Weiss, S.R.B. (1985). Normative data for pigeon vision. Vision Research *25*, 1525–1527.

Hodos, W., Potocki, A., Ghim, M.M., and Gaffney, M. (2003). Temporal modulation of spatial contrast vision in pigeons (Columba livia). Vision Research *43*, 761–767.

Igoe, D., Parisi, A., and Carter, B. (2013). Characterization of a Smartphone Camera's Response to Ultraviolet A Radiation. Photochemistry and Photobiology *89*, 215–218.

Jacobs, G.H., Deegan, J.F., Crognale, M.A., and Fenwick, J.A. (1993). Photopigments of dogs and foxes and their implications for canid vision. Visual Neuroscience *10*, 173–180.

Jarvis, J.R., and Wathes, C.M. (2007). On the calculation of optical performance factors from vertebrate spatial contrast sensitivity. Vision Research *47*, 2259–2271.

941 Jensen, J.R. (2009). Remote sensing of the environment: An earth resource perspective 2/e
942 (Pearson Education India).

943 Jones, D.L. (2017). FATHOM: A Matlab toolbox for ecological and oceanographic data analysis
944 (St. Petersburg, FL USA: College of Marine Science, University of South Florida).

945 Jones, C.D., and Osorio, D. (2004). Discrimination of oriented visual textures by poultry chicks.
946 Vision Research *44*, 83–89.

947 Kasparson, A.A., Badridze, J., and Maximov, V.V. (2013). Colour cues proved to be more
948 informative for dogs than brightness. Proceedings of the Royal Society of London B: Biological
949 Sciences *280*, 20131356.

950 Kelber, A. (2016). Colour in the eye of the beholder: receptor sensitivities and neural circuits
951 underlying colour opponency and colour perception. Current Opinion in Neurobiology *41*, 106–
952 112.

953 Kelber, A., and Osorio, D. (2010). From spectral information to animal colour vision:
954 experiments and concepts. Proceedings of the Royal Society of London B: Biological Sciences
955 *277*, 1617–1625.

956 Linberg, K.A., Lewis, G.P., Shaaw, C., Rex, T.S., and Fisher, S.K. (2001). Distribution of S- and
957 M-cones in normal and experimentally detached cat retina. Journal of Comparative Neurology
958 *430*, 343–356.

959 Lind, O. (2016). Colour vision and background adaptation in a passerine bird, the zebra finch
960 (Taeniopygia guttata). Royal Society Open Science *3*, 160383.

961 Lind, O., Karlsson, S., and Kelber, A. (2013). Brightness Discrimination in Budgerigars
962 (Melopsittacus undulatus). PLOS ONE *8*, e54650.

963 Lind, O., Chavez, J., and Kelber, A. (2014). The contribution of single and double cones to
964 spectral sensitivity in budgerigars during changing light conditions. J Comp Physiol A *200*, 197–
965 207.

966 Loss, S., Will, T., and Marra, P. (2015). Direct mortality of birds from anthropogenic causes.
967 Annual Review of Ecology, Evolution, and Systematics *46*, 99–120.

968 Lovell, P.G., Ruxton, G.D., Langridge, K.V., and Spencer, K.A. (2013). Egg-Laying Substrate
969 Selection for Optimal Camouflage by Quail. Current Biology *23*, 260–264.

970 Loyau, A., Gomez, D., Moureau, B., Théry, M., Hart, N.S., Jalme, M.S., Bennett, A.T.D., and
971 Sorci, G. (2007). Iridescent structurally based coloration of eyespots correlates with mating
972 success in the peacock. Behav Ecol *18*, 1123–1131.

973 Maertens, M., and Wichmann, F.A. (2013). When luminance increment thresholds depend on
974 apparent lightness. Journal of Vision *13*, 21–21.

975 Maia, R., and White, T.E. (2018). Comparing colors using visual models. Behav Ecol *29*, 649–
976 659.

977 Melin, A.D., Kline, D.W., Hiramatsu, C., and Caro, T. (2016). Zebra Stripes through the Eyes of
978 Their Predators, Zebras, and Humans. PLOS ONE *11*, e0145679.

979 Miller, P.E., and Murphy, C.J. (1995). Vision in dogs. Journal-American Veterinary Medical
980 Association *207*, 1623–1634.

981 Møller, A.P., and Nielsen, J.T. (2006). Prey vulnerability in relation to sexual coloration of prey.
982 Behav Ecol Sociobiol *60*, 227–233.

983 Møller, A.P., Erritzøe, J., and Nielsen, J.T. (2010). Causes of interspecific variation in
984 susceptibility to cat predation on birds. Chinese Birds *1*, 97–111.

985 Mondal, K., Gupta, S., Qureshi, Q., and Sankar, K. (2011). Prey selection and food habits of
986 leopard (Panthera pardus fusca) in Sariska Tiger Reserve, Rajasthan, India. Mammalia *75*,
987 201–205.

988 Montgomerie, R., Lyon, B., and Holder, K. (2001). Dirty ptarmigan: behavioral modification of
989 conspicuous male plumage. Behav Ecol *12*, 429–438.

990 Mowat, F.M., Petersen-Jones, S.M., Williamson, H., Williams, D.L., Luthert, P.J., Ali, R.R., and
991 Bainbridge, J.W. (2008). Topographical characterization of cone photoreceptors and the area
992 centralis of the canine retina. Mol Vis *14*, 2518–2527.

993 Neitz, J., Geist, T., and Jacobs, G.H. (1989). Color vision in the dog. Visual Neuroscience *3*,
994 119–125.

995 Nokelainen, O., Hubbard, N., Lown, A.E., Wood, L.E., and Stevens, M. (2017). Through
996 predators' eyes: phenotype–environment associations in shore crab coloration at different
997 spatial scales. Biol J Linn Soc *122*, 738–751.

998 Olsson, P., Lind, O., and Kelber, A. (2015). Bird colour vision: behavioural thresholds reveal
999 receptor noise. Journal of Experimental Biology *218*, 184–193.

1000 Olsson, P., Wilby, D., and Kelber, A. (2016). Quantitative studies of animal colour constancy:
1001 using the chicken as model. Proc. R. Soc. B *283*, 20160411.

1002 Olsson, P., Lind, O., and Kelber, A. (2017). Chromatic and achromatic vision: parameter choice
1003 and limitations for reliable model predictions. Behav Ecol *29*, 273–282.

1004 Osorio, D., and Ham, A.D. (2002). Spectral reflectance and directional properties of structural
1005 coloration in bird plumage. Journal of Experimental Biology *205*, 2017–2027.

1006 Osorio, D., and Vorobyev, M. (2005). Photoreceptor spectral sensitivities in terrestrial animals:
1007 adaptations for luminance and colour vision. Proceedings of the Royal Society of London B:
1008 Biological Sciences *272*, 1745–1752.

1009 Outomuro, D., Söderquist, L., Johansson, F., Ödeen, A., and Nordström, K. (2017). The price of
1010 looking sexy: visual ecology of a three-level predator–prey system. Functional Ecology *31*, 707–
1011 718.

1012 Pascual, J., Senar, J.C., and Domènech, J. (2014). Plumage brightness, vigilance, escape
1013 potential, and predation risk in male and female Eurasian Siskins (Spinus spinus). The Auk *131*,
1014 61–72.

1015 Pessoa, D.M.A., Maia, R., Ajuz, R.C. de A., Moraes, P.Z.P.M.R.D., Spyrides, M.H.C., and
1016 Pessoa, V.F. (2014). The adaptive value of primate color vision for predator detection. American
1017 Journal of Primatology *76*, 721–729.

1018 Peters, R., Hemmi, J., and Zeil, J. (2008). Image motion environments: background noise for
1019 movement-based animal signals. J Comp Physiol A *194*, 441–456.

1020 Petrie, M. (1992). Peacocks with low mating success are more likely to suffer predation. Animal
1021 Behaviour *44*, 585–586.

1022 Petrie, M., Tim, H., and Carolyn, S. (1991). Peahens prefer peacocks with elaborate trains.
1023 Animal Behaviour *41*, 323–331.

1024 Pike, T.W. (2018). Quantifying camouflage and conspicuousness using visual salience.
1025 Methods in Ecology and Evolution *9*, 1883–1895.

1026 Pretterer, G., Bubna-Littitz, H., Windischbauer, G., Gabler, C., and Griebel, U. (2004).
1027 Brightness discrimination in the dog. Journal of Vision *4*, 10–10.

1028 Prutchi, D. (2016). Exploring Ultraviolet Photography (Amherst Media).

1029 Ranjith, V., and Jose, B. (2016). Habitat preference of Indian peafowl (Pavo cristatus) in
1030 selected areas of Palakkad district, Kerala, India. Current Science *110*, 2177–2182.

1031 Renoult, J.P., Kelber, A., and Schaefer, H.M. (2015). Colour spaces in ecology and evolutionary
1032 biology. Biological Reviews *92*, 292–315.

1033 Ridley, M.W., Lelliott, A.D., and Rands, M.R.W. (1984). The courtship display of feral peafowl.
1034 Journal of World Pheasant Association *9*, 57–68.

1035 Robbins, C.S. (1981). Effect of time of day on bird activity. Studies in Avian Biology *6*, 275–286.

1036 Ruxton, G.D., Sherratt, T.N., and Speed, M.P. (2004). Avoiding Attack: The Evolutionary
1037 Ecology of Crypsis, Warning Signals and Mimicry (OUP Oxford).

1038 Sharma, I.K. (1974). Ecological Studies of the Plumes of the Peacock (Pavo cristatus). The
1039 Condor *76*, 344–346.

1040 Shawkey, M.D., and Hill, G.E. (2005). Carotenoids need structural colours to shine. Biology
1041 Letters *1*, 121–124.

1042 Sicsú, P., Manica, L.T., Maia, R., and Macedo, R.H. (2013). Here comes the sun: multimodal
1043 displays are associated with sunlight incidence. Behav Ecol Sociobiol *67*, 1633–1642.

1044 Siddiqi, A., Cronin, T.W., Loew, E.R., Vorobyev, M., and Summers, K. (2004). Interspecific and
1045 intraspecific views of color signals in the strawberry poison frog Dendrobates pumilio. Journal of
1046 Experimental Biology *207*, 2471–2485.

de Silva, P.K., Santiapillai, C., and Dissanayake, S. (1996). Some aspects of the population ecology of the blue peafowl, Pavo cristatus, in Ruhuna National Park, Sri Lanka. Journal of South Asian Natural History *2*, 113–126.

Somppi, S., Törnqvist, H., Kujala, M.V., Hänninen, L., Krause, C.M., and Vainio, O. (2016). Dogs Evaluate Threatening Facial Expressions by Their Biological Validity – Evidence from Gazing Patterns. PLOS ONE *11*, e0143047.

Spitschan, M., Aguirre, G.K., Brainard, D.H., and Sweeney, A.M. (2016). Variation of outdoor illumination as a function of solar elevation and light pollution. Scientific Reports *6*, 26756.

Stevens, M., and Cuthill, I.C. (2007). Hidden Messages: Are Ultraviolet Signals a Special Channel in Avian Communication? BioScience *57*, 501–507.

Stevens, M., and Merilaita, S. (2011). Animal Camouflage: Mechanisms and Function (Cambridge University Press).

Stevens, M., and Ruxton, G.D. (2014). Do animal eyespots really mimic eyes? Current Zoology *60*, 26–36.

Stevens, M., Párraga, C.A., Cuthill, I.C., Partridge, J.C., and Troscianko, T.S. (2007). Using digital photography to study animal coloration. Biol J Linn Soc *90*, 211–237.

Stoddard, M.C., and Prum, R.O. (2008). Evolution of Avian Plumage Color in a Tetrahedral Color Space: A Phylogenetic Analysis of New World Buntings. The American Naturalist *171*, 755–776.

Stoddard, M.C., and Stevens, M. (2010). Pattern mimicry of host eggs by the common cuckoo, as seen through a bird's eye. Proceedings of the Royal Society of London B: Biological Sciences rspb20092018.

Stoddard, M.C., Kupán, K., Eyster, H.N., Rojas-Abreu, W., Cruz-López, M., Serrano-Meneses, M.A., and Küpper, C. (2016). Camouflage and Clutch Survival in Plovers and Terns. Scientific Reports *6*, 32059.

Stoddard, M.C., Miller, A.E., Eyster, H.N., and Akkaynak, D. (2019). I see your false colours: how artificial stimuli appear to different animal viewers. Interface Focus *9*, 20180053.

Stuart-Fox, D. (2018). Opening the "black box" of modeling animal color vision: a comment on Olsson et al. Behav Ecol *29*, 284–284.

Sumner, P., and Mollon, J.D. (2003). Colors of primate pelage and skin: Objective assessment of conspicuousness. American Journal of Primatology *59*, 67–91.

Talha, M.M.H., Mia, M.M., and Momu, J.M. (2018). Morphometric, productive and reproductive traits of Indian peafowl (Pavo cristatus) in Bangladesh. International Journal of Development Research *8*, 19039–19043.

Thavarajah, N.K., Tickle, P.G., Nudds, R.L., and Codd, J.R. (2016). The peacock train does not handicap cursorial locomotor performance. Scientific Reports *6*, 36512.

1083 Théry, M., Debut, M., Gomez, D., and Casas, J. (2005). Specific color sensitivities of prey and
1084 predator explain camouflage in different visual systems. Behav Ecol *16*, 25–29.

1085 Tinbergen, J., Wilts, B.D., and Stavenga, D.G. (2013). Spectral tuning of Amazon parrot feather
1086 coloration by psittacofulvin pigments and spongy structures. Journal of Experimental Biology
1087 jeb.091561.

1088 Toral, G.M., Figuerola, J., and Negro, J.J. (2008). Multiple ways to become red: Pigment
1089 identification in red feathers using spectrometry. Comparative Biochemistry and Physiology Part
1090 B: Biochemistry and Molecular Biology *150*, 147–152.

1091 Trivedi, P., and Johnsingh, A.J.T. (1996). Roost selection by Indian Peafowl (Pavo cristatus) in
1092 Gir Forest, India. Journal of the Bombay Natural Histroy Society *93*, 25–29.

1093 Troscianko, J., and Stevens, M. (2015). Image calibration and analysis toolbox – a free software
1094 suite for objectively measuring reflectance, colour and pattern. Methods in Ecology and
1095 Evolution *6*, 1320–1331.

1096 Troscianko, J., Wilson-Aggarwal, J., Griffiths, D., Spottiswoode, C.N., and Stevens, M. (2017).
1097 Relative advantages of dichromatic and trichromatic color vision in camouflage breaking. Behav
1098 Ecol *28*, 556–564.

1099 Van Wijk, S., Bélisle, M., Garant, D., and Pelletier, F. (2016). A reliable technique to quantify the
1100 individual variability of iridescent coloration in birds. Journal of Avian Biology *47*, 227–234.

1101 Vehrencamp, S.L., Bradbury, J.W., and Gibson, R.M. (1989). The energetic cost of display in
1102 male sage grouse. Animal Behaviour *38*, 885–896.

1103 Vogt, M.C., and Vogt, M.E. (2016). RESEARCH ARTICLE: Near-Remote Sensing of Water
1104 Turbidity Using Small Unmanned Aircraft Systems. Environmental Practice *18*, 18–31.

1105 Vorobyev, M., and Osorio, D. (1998). Receptor noise as a determinant of colour thresholds.
1106 Proceedings of the Royal Society of London B: Biological Sciences *265*, 351–358.

1107 Vukusic, P., and Stavenga, D.G. (2009). Physical methods for investigating structural colours in
1108 biological systems. Journal of The Royal Society Interface *6*, S133–S148.

1109 Walther, B.A. (2003). Do peacocks devote maintenance time to their ornamental plumage?
1110 Time budgets of male blue peafowl Pavo cristatus. Lundiana *4*, 149–154.

1111 Wilkinson, H., Thavarajah, N., and Codd, J. (2015). The metabolic cost of walking on an incline
1112 in the Peacock (Pavo cristatus). PeerJ *3*, e987.

1113 Yasmin, S., and Yahya, H.S.A. (2000). Group size and vigilance in Indian peafowl. Journal of
1114 the Bombay Natural History Society *97*, 425–428.

1115 Yorzinski, J.L., Patricelli, G.L., Babcock, J.S., Pearson, J.M., and Platt, M.L. (2013). Through
1116 their eyes: selective attention in peahens during courtship. Journal of Experimental Biology *216*,
1117 3035–3046.

Yorzinski, J.L., Platt, M.L., and Adams, G.K. (2015). Eye-spots in Lepidoptera attract attention in humans. R Soc Open Sci *2*.

Yoshioka, S., and Kinoshita, S. (2002). Effect of macroscopic structure in iridescent color of the peacock feathers. Forma-Tokyo *17*, 169–181.

Yun, H.S., Park, S.H., Kim, H.-J., Lee, W.D., Lee, K.D., Hong, S.Y., and Jung, G.H. (2016). Use of Unmanned Aerial Vehicle for Multi-temporal Monitoring of Soybean Vegetation Fraction. Journal of Biosystems Engineering *41*, 126–137.

Zahavi, A. (1975). Mate selection—A selection for a handicap. Journal of Theoretical Biology *53*, 205–214.

Zuiderveld, K. (1994). Contrast Limited Adaptive Histogram Equalization. Graphics Gems 474–485.

Supporting information captions

S1 Appendix. Predators of Indian peafowl.

S2 Appendix. Species of plants used for background foliage in multispectral images.

S3 Appendix. Methods for spatially filtering multispectral images to account for visual acuity effects at varying viewing distances.

S1 Fig. Multispectral camera specifications: image sensor spectral response and filter transmission spectra.

S2 Fig. Reflectance spectroscopy apparatus and multispectral camera filming setup.

S3 Fig. Various green leaves imaged and analyzed for comparison with feather samples and the saucer magnolia leaves used as a background.

S4 Fig. Model train false color images.

S5 Fig. Model peacock train edge detected images.

S1 Dataset. Color and brightness contrast data and PERMANOVA pseudo-F and P values for Indian peacock eyespot feathers

S2 Dataset. Color and brightness contrast data and PERMANOVA pseudo-F and P values for model Indian peacock train

S3 Dataset. Color and brightness contrast data and PERMANOVA pseudo-F and P values for Indian peacock blue body feathers

S4 Dataset. Color and brightness contrast data and PERMANOVA pseudo-F and P values for parrot feathers

S5 Dataset. Granularity and edge-detection visual texture data for model Indian peacock train

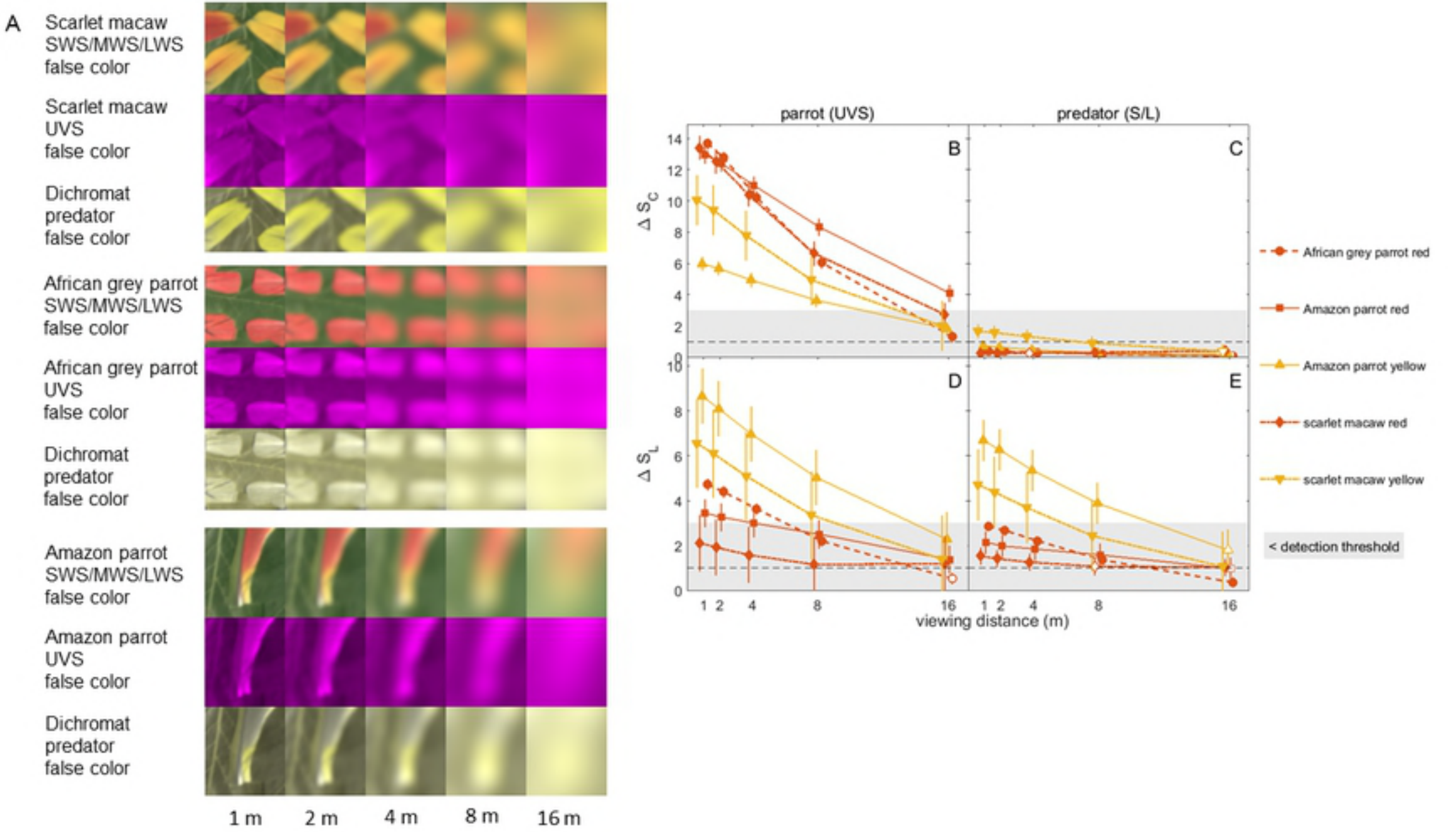
A
Scarlet macaw
SWS/MWS/LWS
false color
Scarlet macaw
UVS
false color
Dichromat
predator
false color
African grey parrot
SWS/MWS/LWS
false color
African grey parrot
UVS
false color
Dichromat
predator
false color
Amazon parrot
SWS/MWS/LWS
false color
Amazon parrot
UVS
false color
Dichromat
predator
false color
1 m
2 m
4 m
8 m
16 m
parrot (UVS)
predator (S/L)
B
C
D
E
ΔS_C
ΔS_L
viewing distance (m)
African grey parrot red
Amazon parrot red
Amazon parrot yellow
scarlet macaw red
scarlet macaw yellow
< detection threshold

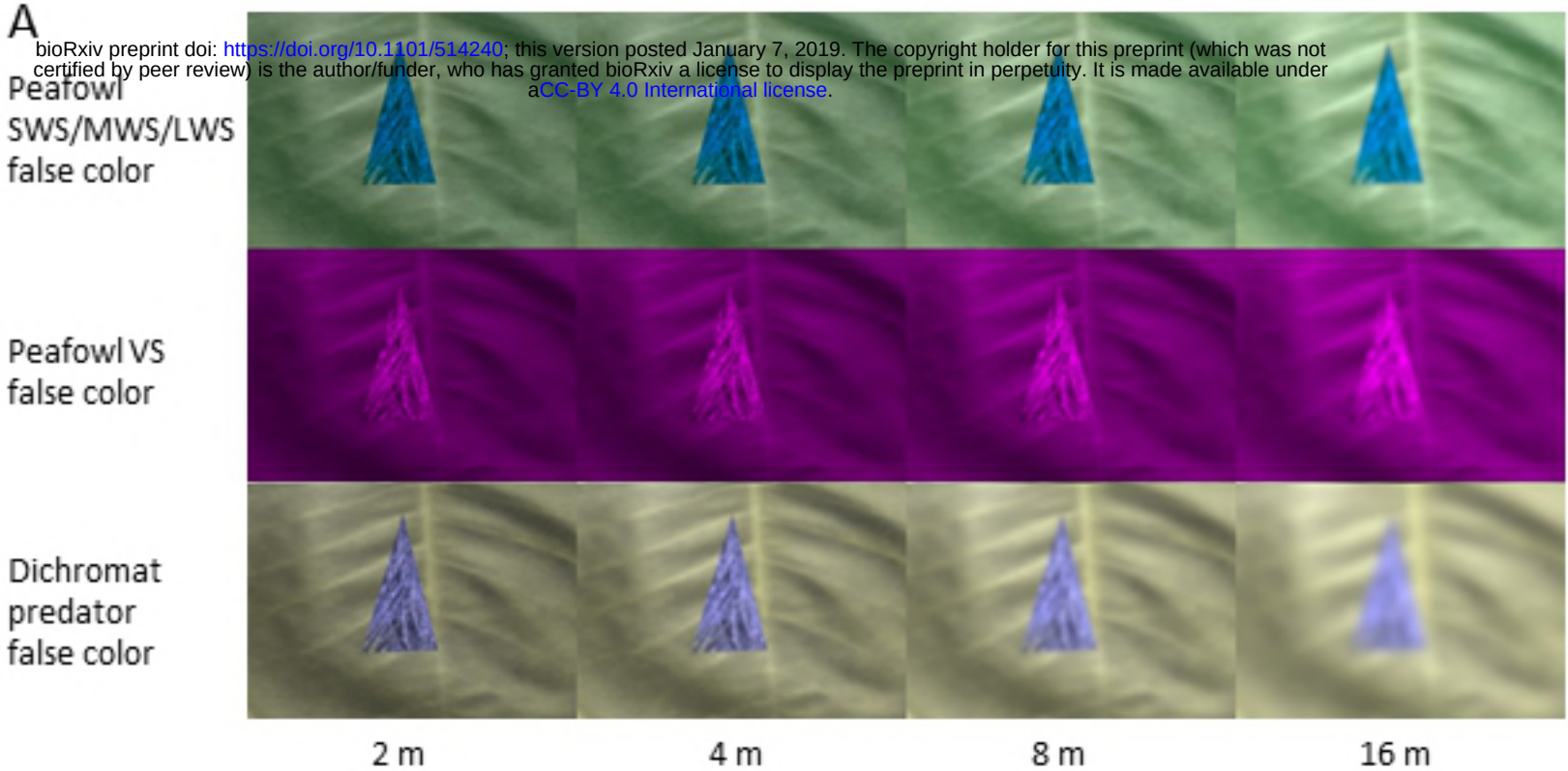

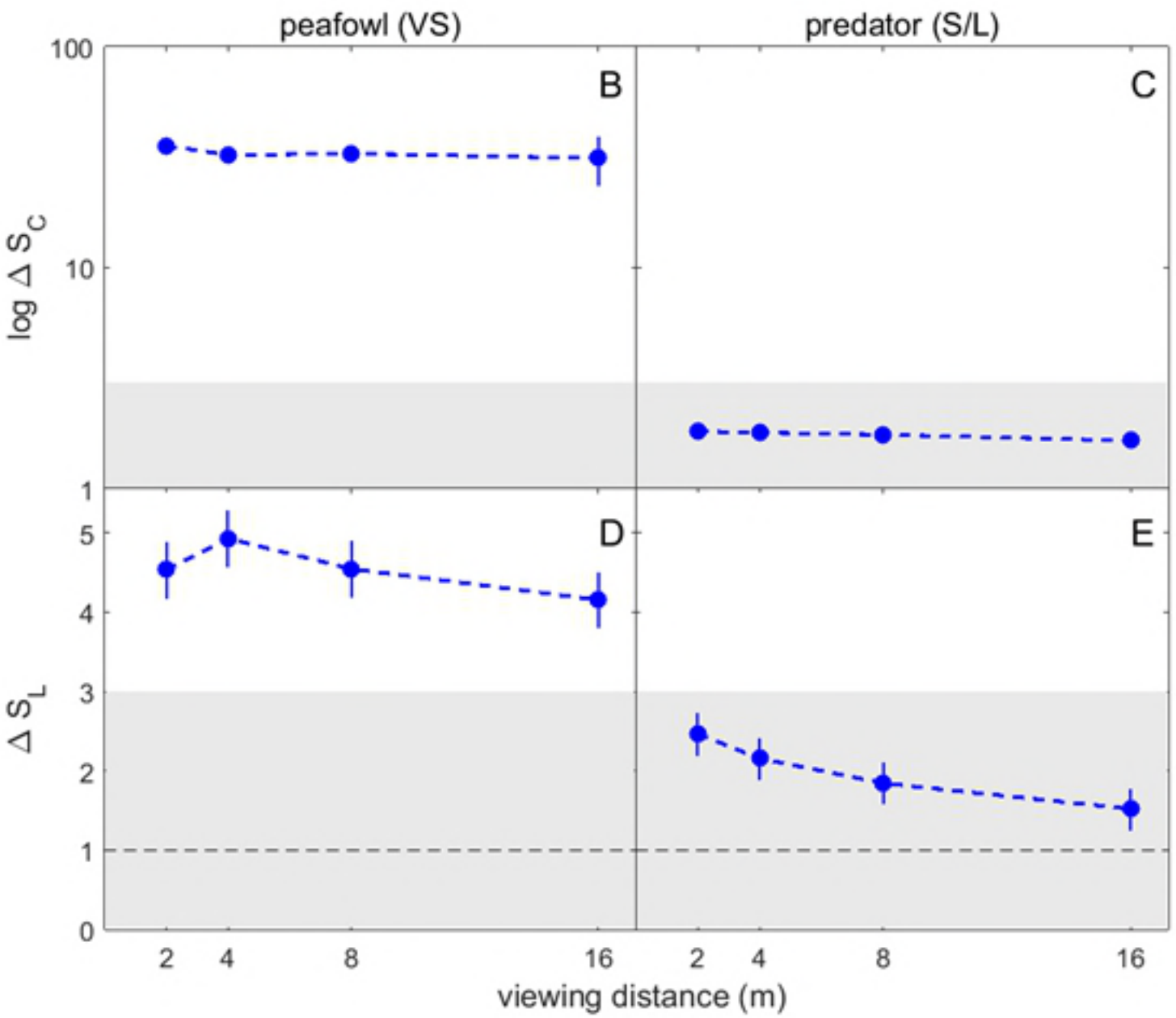

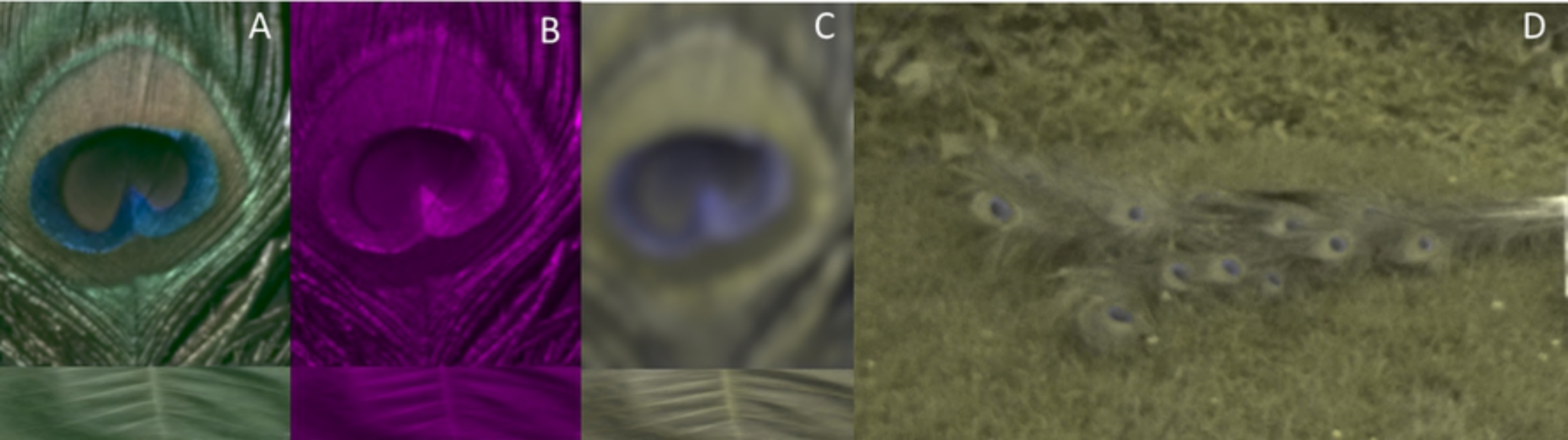
A
B
C
D

A

Peafowl SWS/MWS/LWS false color

Peafowl VS false color

Dichromat predator false color

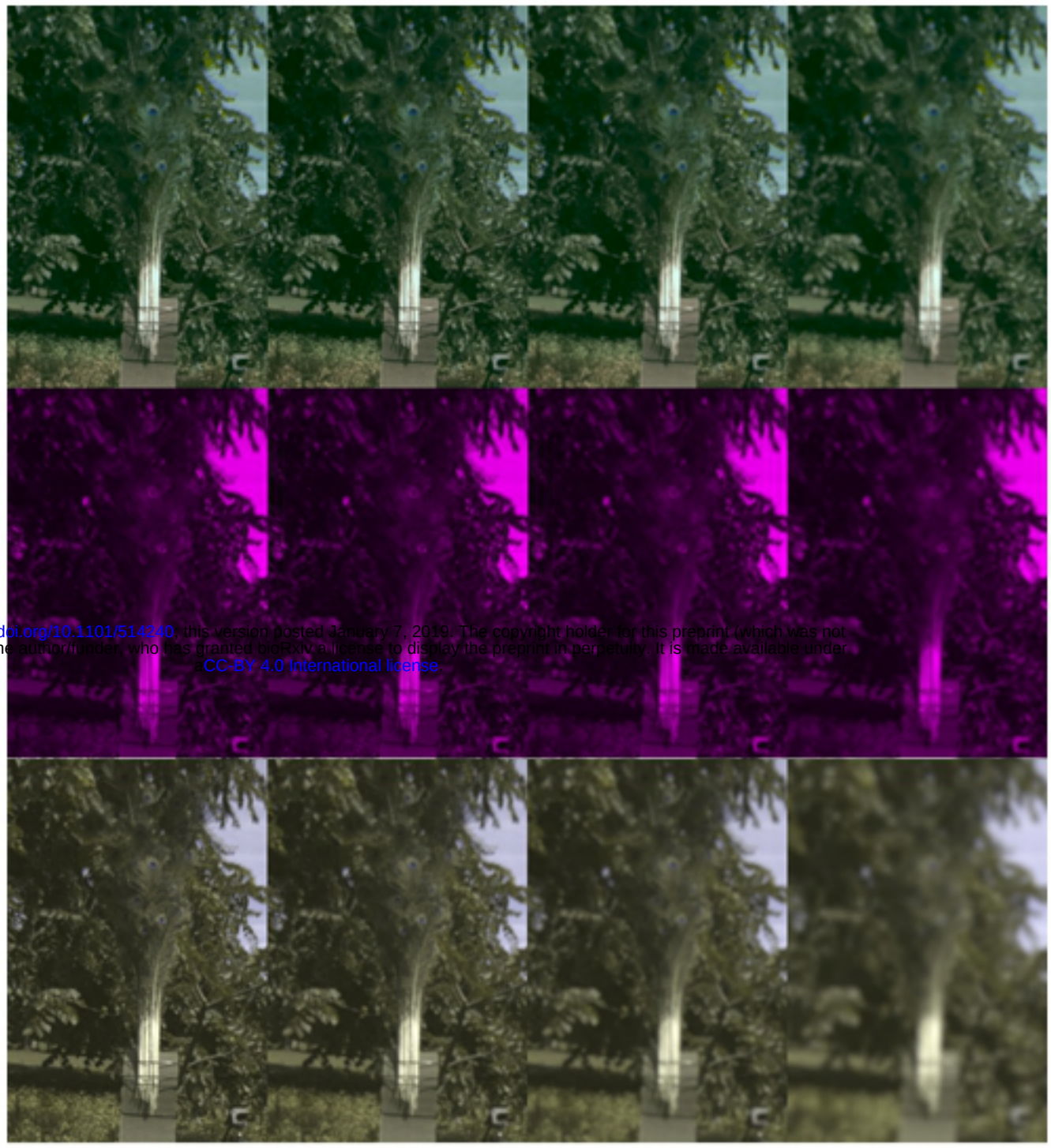

2 m 4 m 8 m 16 m

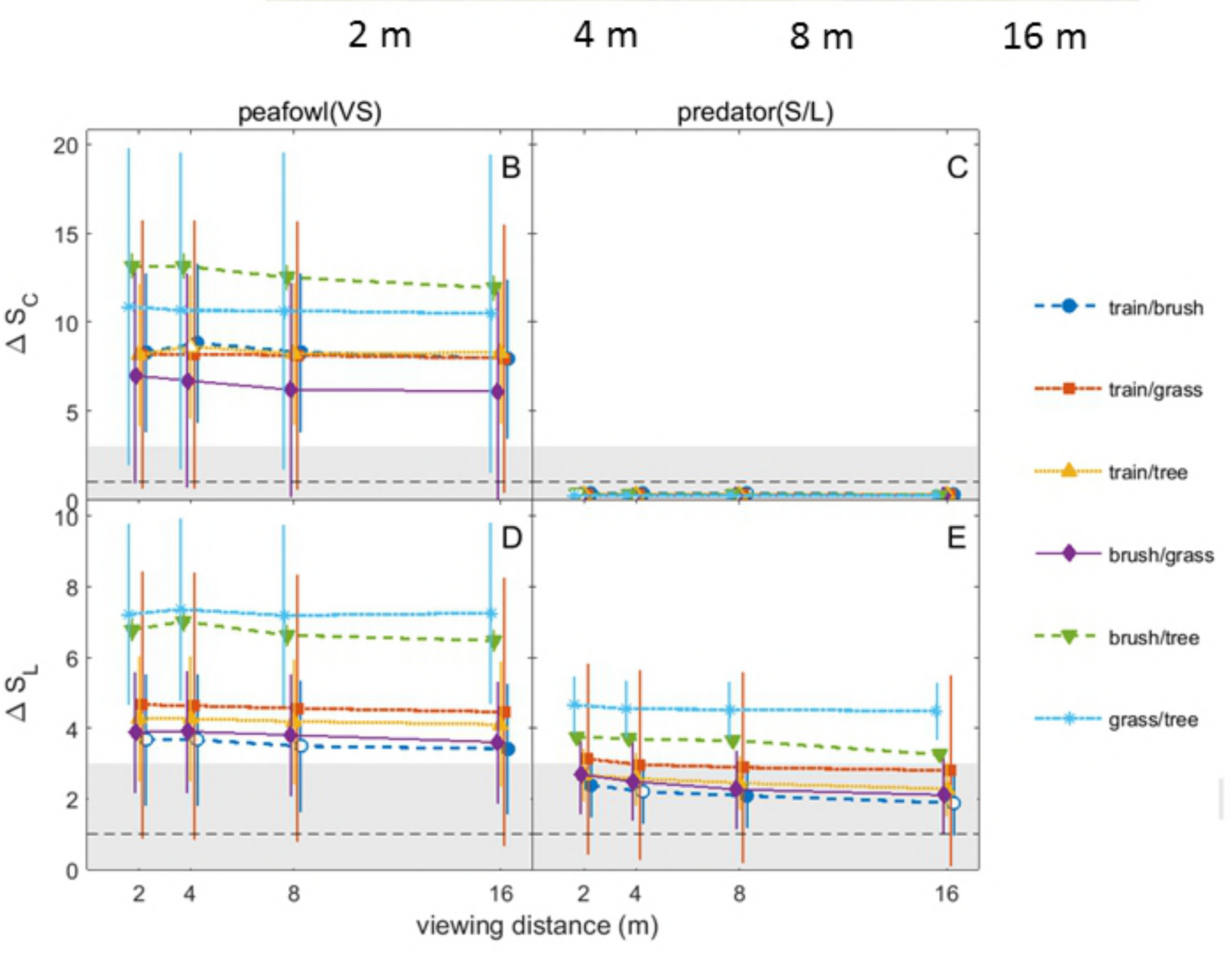

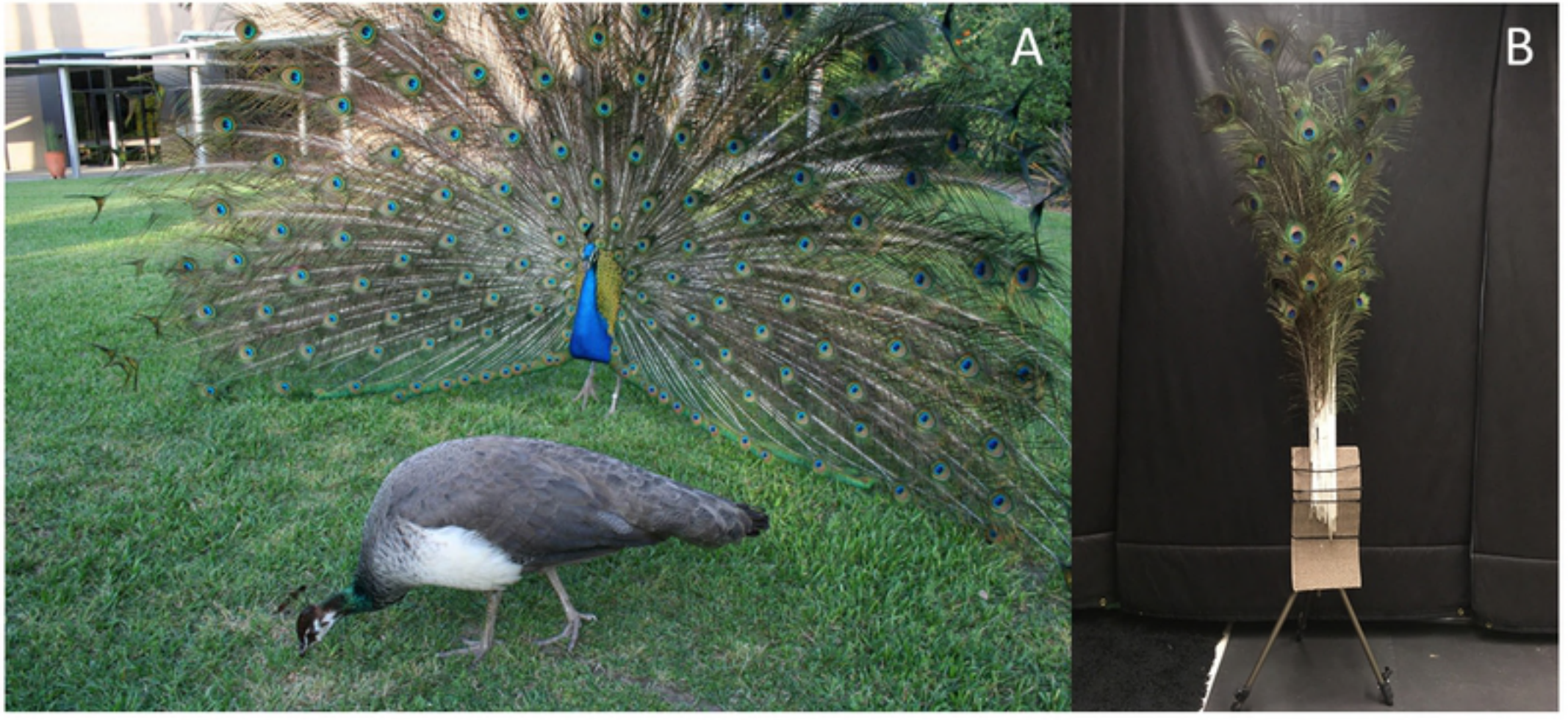
A
B

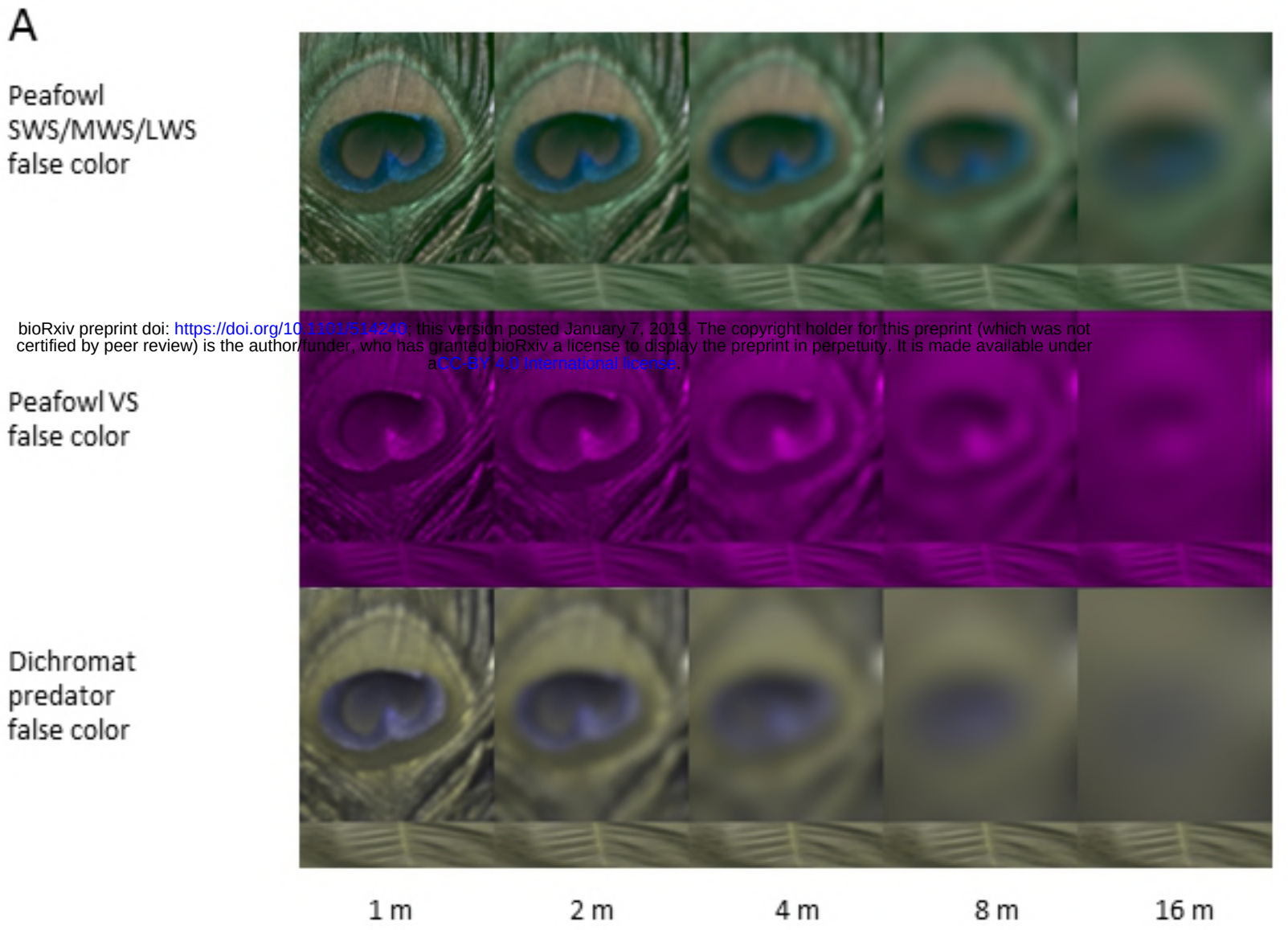

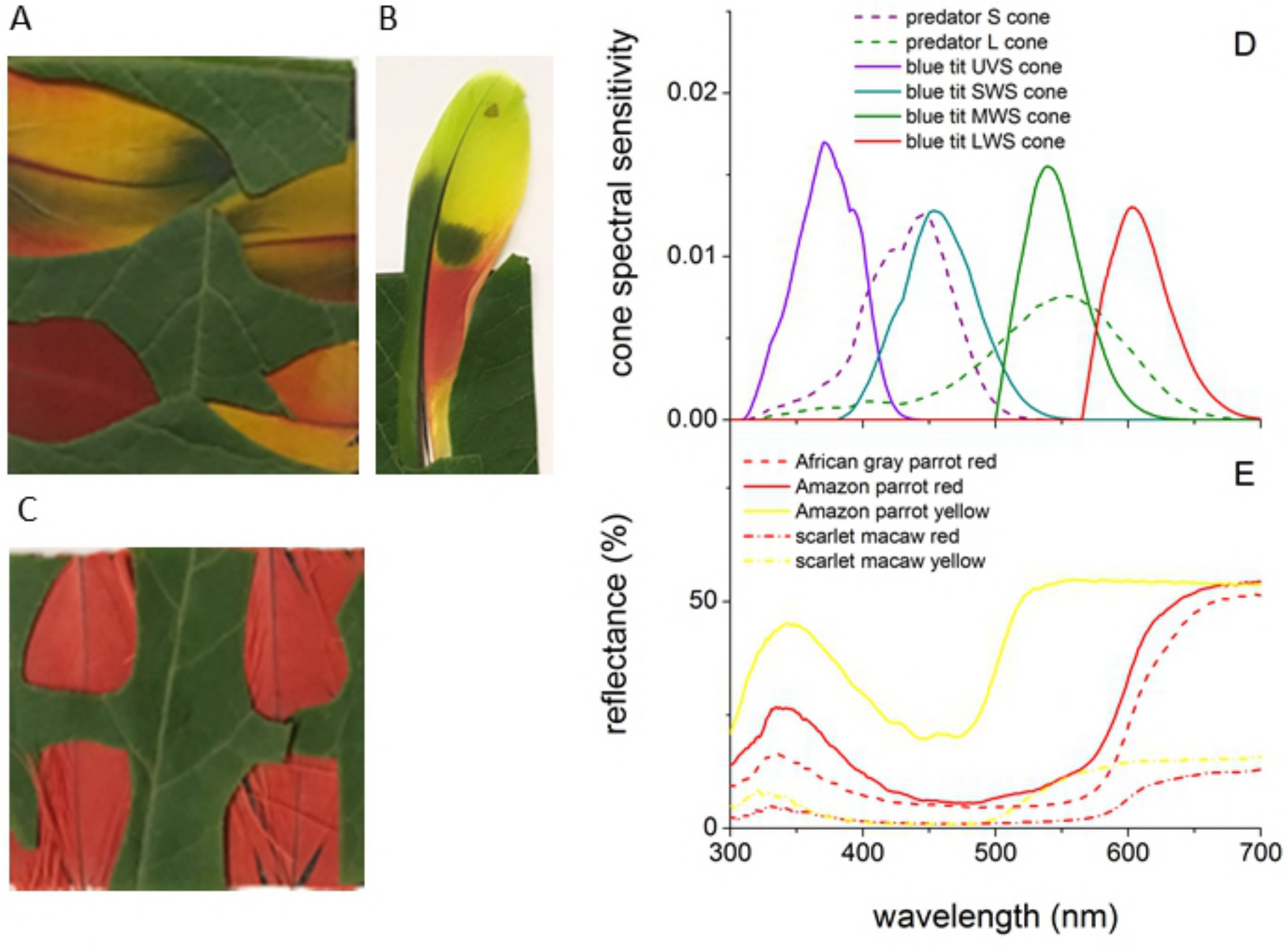
A
B
C
D
predator S cone
predator L cone
blue tit UVS cone
blue tit SWS cone
blue tit MWS cone
blue tit LWS cone
cone spectral sensitivity
0.02
0.01
0.00
E
African gray parrot red
Amazon parrot red
Amazon parrot yellow
scarlet macaw red
scarlet macaw yellow
reflectance (%)
50
0
300
400
500
600
700
wavelength (nm)

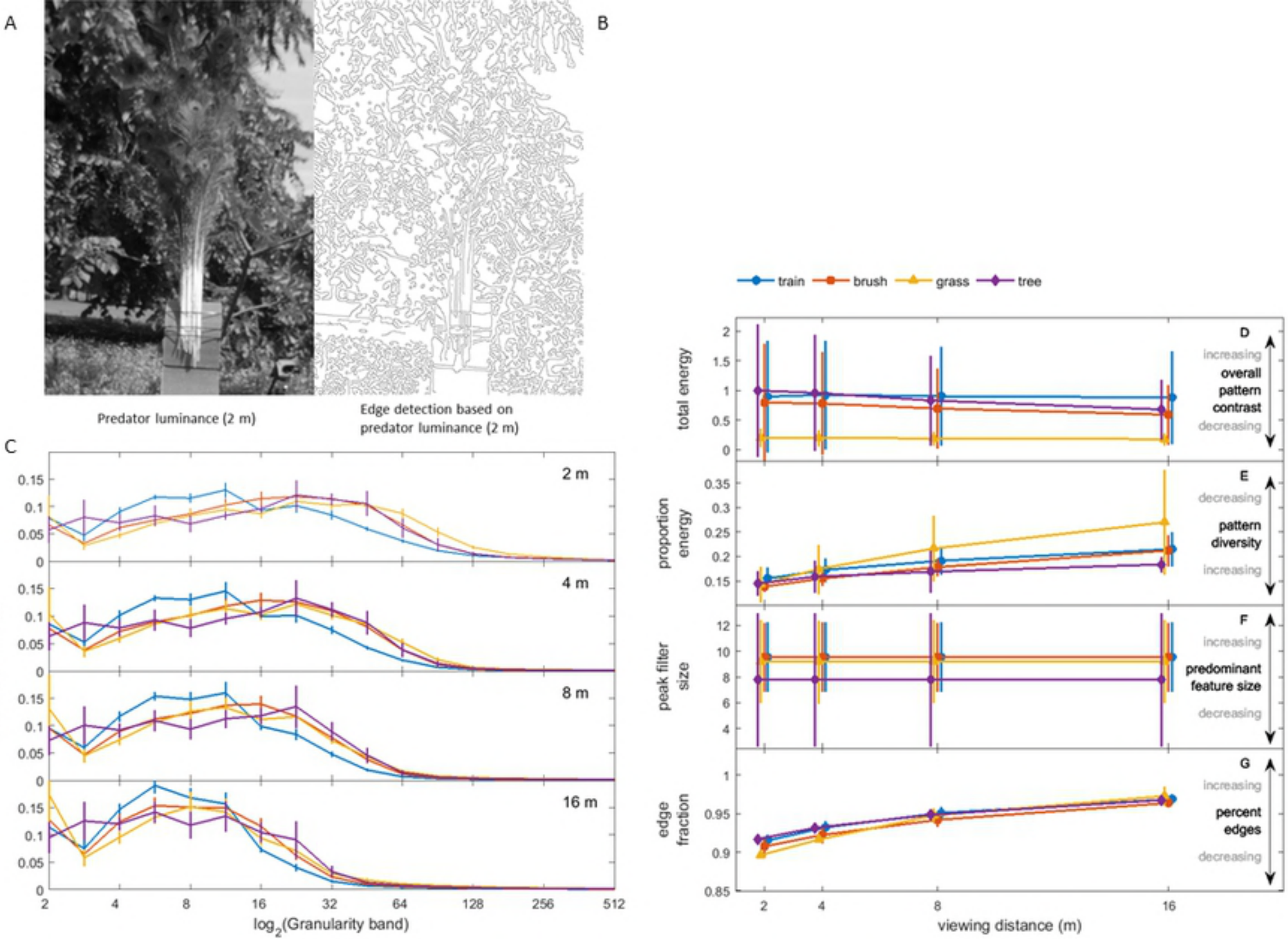
A
B
Predator luminance (2 m)
Edge detection based on predator luminance (2 m)
C
2 m
4 m
8 m
16 m
Normalized energy
log2(Granularity band)
train
brush
grass
tree
D
total energy
increasing
overall pattern contrast
decreasing
E
proportion energy
decreasing
pattern diversity
increasing
F
peak filter size
increasing
predominant feature size
decreasing
G
edge fraction
increasing
percent edges
decreasing
viewing distance (m)

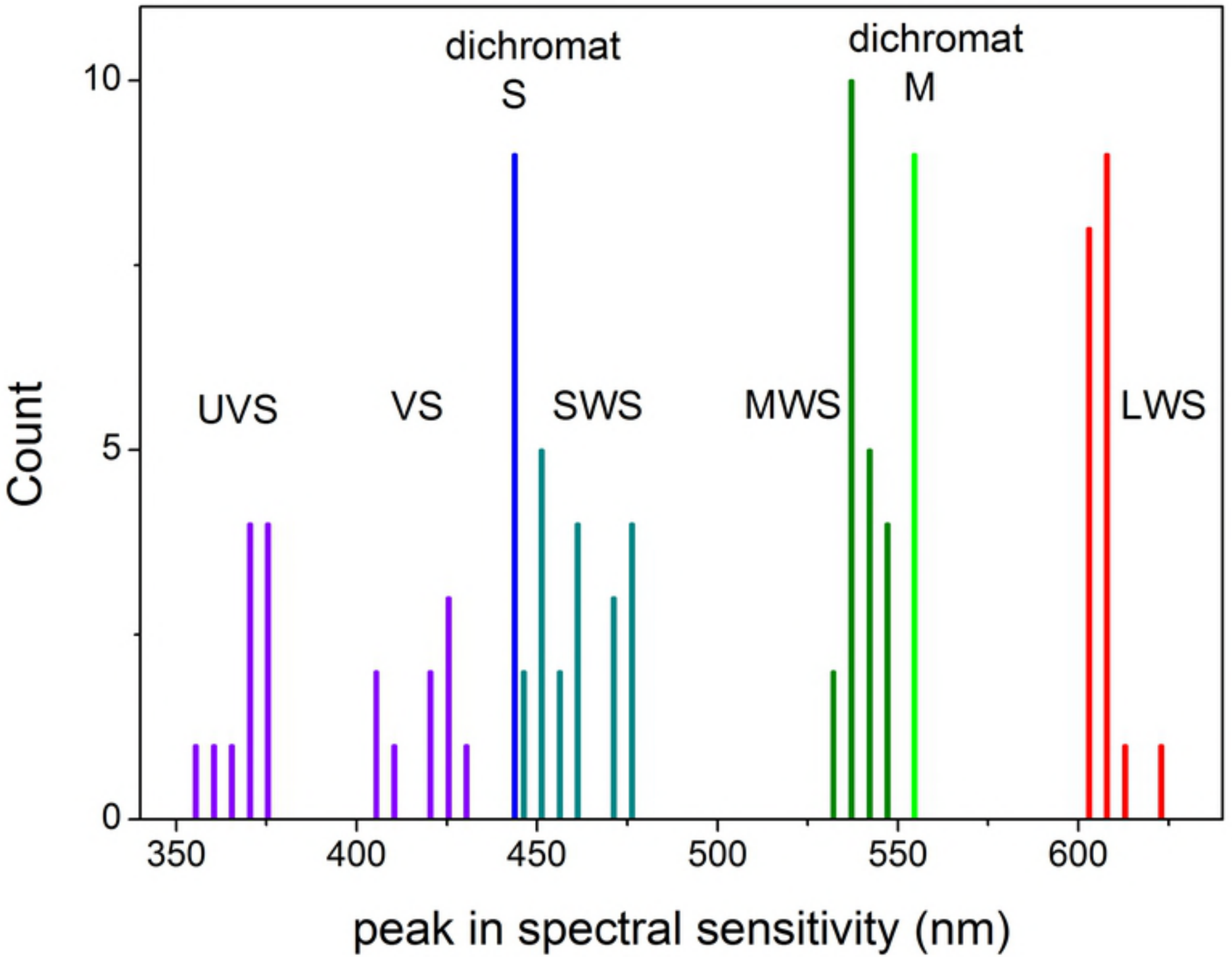
dichromat
S
dichromat
M
UVS
VS
SWS
MWS
LWS
Count
10
5
0
350
400
450
500
550
600
peak in spectral sensitivity (nm)

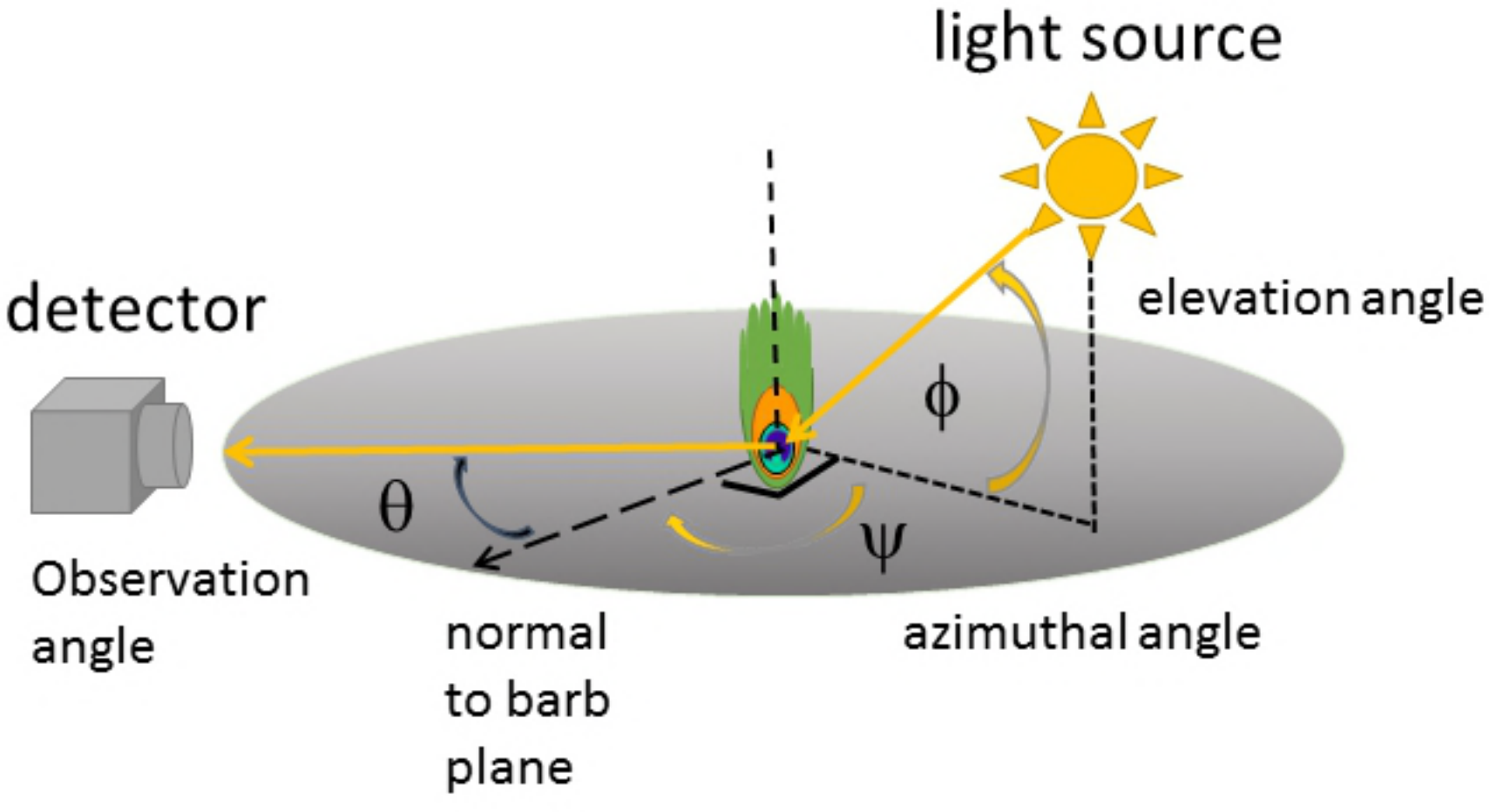
light source
detector
elevation angle
ϕ
θ
ψ
Observation angle
normal to barb plane
azimuthal angle

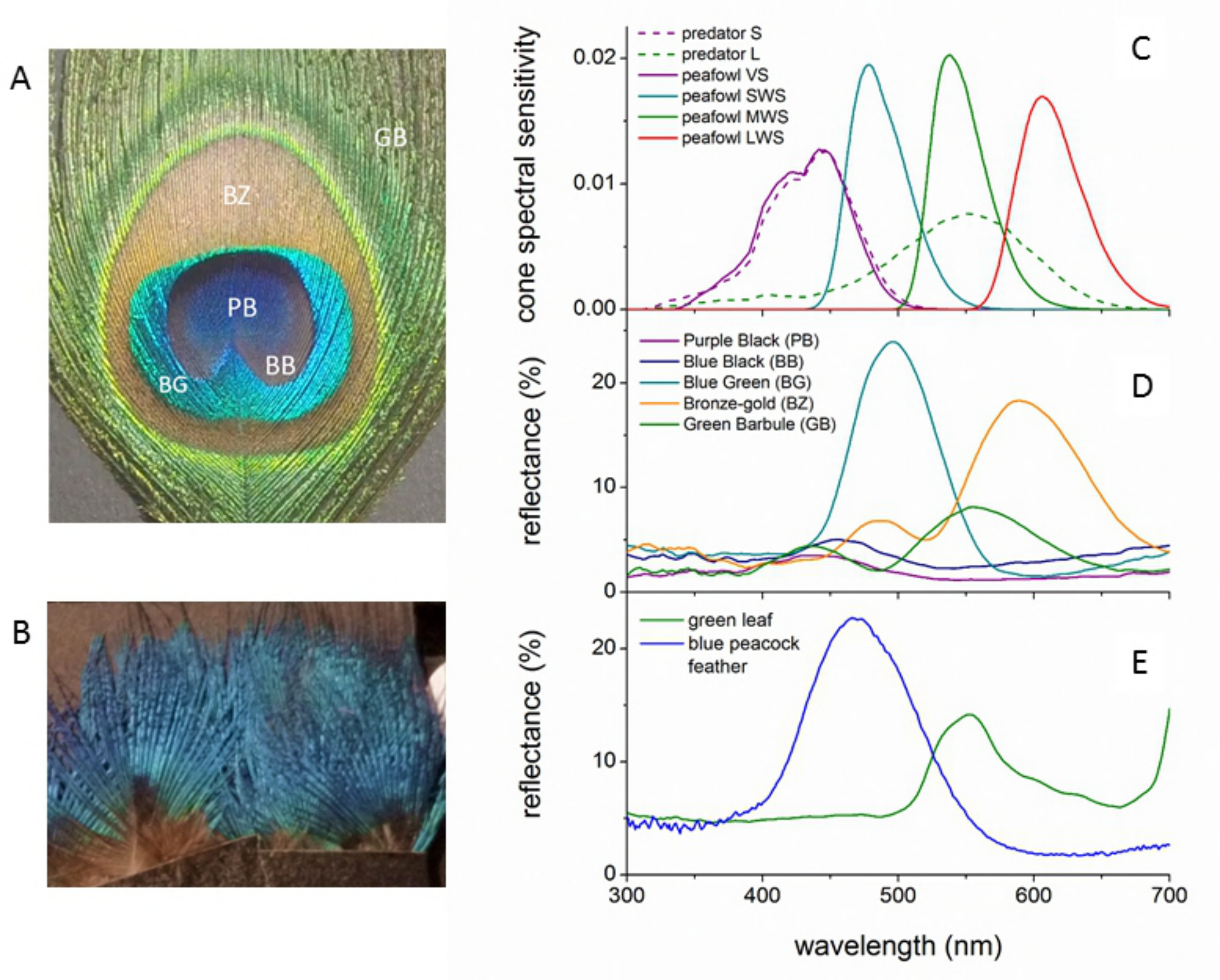
A
GB
BZ
PB
BB
BG
B
C
predator S
predator L
peafowl VS
peafowl SWS
peafowl MWS
peafowl LWS
cone spectral sensitivity
0.02
0.01
0.00
D
Purple Black (PB)
Blue Black (BB)
Blue Green (BG)
Bronze-gold (BZ)
Green Barbule (GB)
reflectance (%)
20
10
0
E
green leaf
blue peacock feather
reflectance (%)
20
10
0
300
400
500
600
700
wavelength (nm)